IEEE Transactions on Robotics (T-RO) paper, presented at ICRA 2023, London, UK. Cite as T-RO paper.

Reduced Euler-Lagrange Equations of Floating-base Robots: Computation, Properties & Applications

Hrishik Mishra, Gianluca Garofalo, Alessandro M. Giordano, Marco De Stefano, Christian Ott, *Senior Member, IEEE* and Andreas Kugi, *Senior Member, IEEE*

***Abstract*—At first glance, a Floating-base Robotic System is a kinematic chain, and its equations of motion are described by the inertia-coupled dynamics of its shape and movable base. However, the dynamics embody an additional structure due to the momentum evolution, which acts as a velocity constraint. In prior works of robot dynamics, matrix transformations of the dynamics revealed a block-diagonal inertia. However, the structure of the transformed matrix of Coriolis/Centrifugal (CC) terms was not examined, and is the primary contribution of this paper. To this end, we simplify the CC terms from robot dynamics and derive the analogous terms from geometric mechanics. Using this interdisciplinary link, we derive a two-part structure of the CC matrix, in which each partition is iteratively computed using a self-evident velocity dependency. Through this CC matrix, we reveal a commutative property, the velocity dependencies of the skew-symmetry property, the invariance of the shape dynamics to the basis of momentum, and the curvature as a matrix operator. Finally, we show the application of the proposed CC matrix structure through controller design and locomotion analysis.**

***Index Terms*—Lagrangian Dynamics, Dynamics, Motion Control, Nonholonomic Mechanisms and Systems.**

I. Introduction

A Floating-base Robotic System (FRS) is an articulated robotic mechanism mounted on a movable platform, and is ubiquitous in several domains [1], [2], [3], as shown in Fig. 1. The commonly-known equations of motion for the FRS are the inertia-coupled dynamics of its configuration (FRS-base and shape) velocities. These dynamics are efficiently computed by considering the FRS as a kinematic chain using standard iterative algorithms from the robot dynamics community [4, §9.4]. These equations also exhibit the skew-symmetry (or passivity) property, which is useful for stability analyses in motion control [3]. From the Lagrangian perspective in geometric mechanics, the dynamics above are seen as a set of an Euler-Poincaré equation and an Euler-Lagrange equation, which correspond to the motion of the FRS-base and the shape (joints), respectively. This set is called a system of Hamel's equations [5], [6]. Among kinematic chain systems, the FRS is unique in its well-known property of momentum conservation. In geometric mechanics, this property is modeled as a Pfaffian-like velocity constraint using a quantity called the *mechanical connection* (see [7, Ex. 4]). The FRS is further distinguished by its distinct non-flatness (curvature) of this connection [5], i.e., the constraint is not preserved over a closed path (gait) in shape space. In other words, a gait might cause a net displacement of the FRS-base. In fact, locomotion approaches in geometric mechanics approximate this displacement per gait using area integrals of the curvature [8], [9], [10], [11], [12].

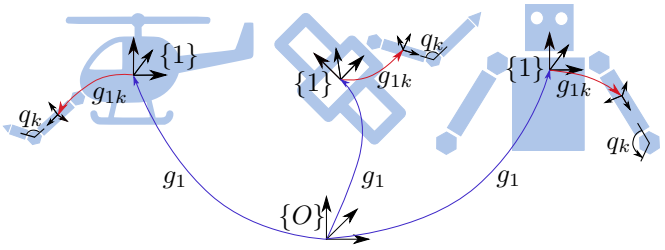

Fig. 1. Floating-base Robotic Systems (FRS) with configuration (g_1, q), where $g_1 \in \mathrm{SE}(3)$ is the pose of the FRS-base frame, $\{1\}$, relative to the inertial frame $\{O\}$, and $q \in \mathbb{R}^n$ are the n-joint positions.

For the dynamics of this class of mechanical systems, the *Reduced Euler Lagrange* (REL) equations [13, §5.3][6, pp. 141] were proposed in the early nineties. In particular, the REL equations consist of momentum and shape variations as an Euler-Poincaré equation and an Euler-Lagrange equation with curvature-related gyroscopic forces, respectively. The structure of the REL equations provide a useful insight into the FRS dynamics through a block-diagonal inertia, the separation of velocity dependencies in the Coriolis/Centrifugal (CC) terms and the apparentness of the curvature form. A first step in this direction by the robot dynamics community was a matrix transformation of the Hamel's equations [1], which revealed the useful block-diagonal inertia property.

However, a direct link between kinematic chain iterative dynamics and REL equations has not been established before. A negative consequence was that only the block-diagonal structure of inertia was exploited, as in [1], [14], whereas the structural properties of the CC matrix were not examined. In fact, the use of matrix transformations resulted in a placeholder CC matrix, which concealed its precise structure. This resulted in a CC matrix, which (a) had an apparent coupling between the shape dynamics and the group variable, (b) lacked a commutative property (like fixed-base robots, see [15]), and (c) did not reveal the FRS curvature. We point out that the curvature computation in FRS locomotion analyses [8], [9], [10], [16] is traditionally performed using numeric or symbolic methods, and an analytical computation method is missing.

H. Mishra, A. M. Giordano, M. De Stefano and C. Ott are with the Institute of Robotics and Mechatronics, German Aerospace Center (DLR), 82234, Wessling, Germany. G. Garofalo is with ABB Corporate Research, 72226, Västerås, Sweden. H. Mishra, C. Ott and A. Kugi are with the Automation and Control Institute (ACIN), Technische Universität (TU) Wien, 1040 Vienna, Austria. A. Kugi is also with the Center for Vision, Automation & Control, Austrian Institute of Technology (AIT) GmbH, 1210 Vienna, Austria. A. M. Giordano is also with the Technical University of Munich, Dept. of Informatics, Munich, Germany. (contact e-mail: hrishik.mishra@dlr.de)

IEEE Transactions on Robotics (T-RO) paper, presented at ICRA 2023, London, UK. Cite as T-RO paper.

The CC matrix of multibody systems is required in applications that include, but are not limited to, motion tracking [17], velocity observers [15] and contact detection [18]. The skew-symmetry of an iteratively computed CC matrix [19] was extended in [20] with Christoffel-symbol consistency. In [21], the CC matrix was structured as the sum of inertia variations relative to time and shape, defined as fundamental matrices. However, prior CC matrix factorizations were limited to configuration velocity dynamics, and the added structure due to velocity constraints, as in the FRS[1], remains unexamined.

To this end, the contributions of this paper are the following. For the REL equations of a FRS, firstly, we propose a novel CC matrix as a sum of two matrices, in which the partitions of each are computed using an iterative expression with a specific velocity dependency. In particular, the first CC matrix depends on the shape velocity, while the second depends on the locked velocity (momentum). We prove that the former CC matrix of block-diagonal terms satisfies the skew-symmetry (passivity) property, while the latter is itself skew-symmetric. Secondly, by extending the notion of fundamental matrices [21] for fixed-base robots to the FRS, we identify the parts of the CC matrix with commutativity. This enables the reordering of velocity arguments in the CC forces for simplification, e.g. in velocity observers, which was previously limited to fixed-base robots [15]. Thirdly, we prove that the shape dynamics is invariant to a transformation of the momentum dynamics, e.g. to a centroidal frame [1]. Fourthly, from the proposed CC matrix, we derive the curvature as an analytic matrix-based expression. Finally, the merit of the proposed structure is demonstrated through the novelty in two FRS applications, namely, observer-based controller design and locomotion analysis. As evidence of the former, we revisit our preliminary work from [22], and marginally extend it to generalize the functionalities from *both*, [14] and [23], while using the proposed CC matrix structure. The control-centric scope of [22], however, did not require computation details of this CC matrix. The work proposed here exhaustively focuses on the derivation of the CC matrix, notably, as an iterative formulation, and its properties, which can appeal to a broad robotics audience. To achieve that, we establish an interdisciplinary link between the forms of REL equations from *both* communities, robot dynamics and geometric mechanics.

The paper is organized as follows. In Sec. II, a summary of useful concepts on $\mathrm{SE}(3)$ motion is given. In Sec. III, the REL equations of motion for the FRS from *both*, robot dynamics and geometric mechanics, are linked. The main result is stated and derived in Sec. IV. Herein, the novel properties of the CC matrix are proved and the closed form expression of curvature is derived. In Sec. V, the two applications benefiting from the proposed CC matrix are provided, of which, the work in [22] is revisited in Sec. V-A. The paper concludes with remarks in Sec. VI. A sectioned Appendix is given to aid the analysis.

II. Modeling motion on $\mathrm{SE}(3)$ group

In this section, rigid-body motion on the $\mathrm{SE}(3)$ group is introduced to provide a foundation for multibody dynamics. For the sake of clarity, the fundamental concepts of the $\mathrm{SE}(3)$ are provided in Appendix A1, and key concepts that are ubiquitous in robot dynamics and geometric mechanics are revisited here. In the following, the pose of a rigid-body is denoted by $g \equiv g(R,p) \in \mathrm{SE}(3)$, where $R \in \mathrm{SO}(3)$ is the rotation matrix and $p \in \mathbb{R}^3$ is the position. The body velocity convention is $\mathcal{V} = \begin{bmatrix}\omega^\top & v^\top\end{bmatrix}^\top$, where ω (v) is the angular (linear, respectively) velocity. A pose between two frames is subscripted with symbols of both frames, e.g. in Fig. 1, the pose of $\{k\}$ relative to $\{1\}$ is g_{1k}. Poses and velocities that are subscripted once are referenced relative to the inertial frame, $\{O\}$, e.g. (g_1, V_1) are the pose and the velocity of the FRS-base, $\{1\}$, relative to $\{O\}$. For simplicity of notation, we indicate the pose argument in the Adjoint operator, Ad, by its ordered frames. e.g. $\mathrm{Ad}_{g_{1k}} = \mathrm{Ad}_{1k}$. Given $A \in \mathbb{R}^{n\times n}$, $A \succ 0$ denotes positive definiteness. An identity matrix of dimension $k \times k$ is denoted by $\mathbb{I}_{k,k}$, and $0_{k,l}$ is a $k \times l$ matrix of zeros, and for $l = 1$, the index is omitted. Henceforth, given $x \in \mathbb{R}^l$, $y \in \mathbb{R}^m$, and $Z \in \mathbb{R}^{l\times m}$, $\langle x, y\rangle_Z = x^\top Z y$.

Rigid-Body Motion: The k^{th} link in Fig. 1 is modeled as a rigid-body with pose $g_k \in \mathrm{SE}(3)$ with reconstruction formula,

$$\text{Kinematics}\Big\{\ \dot{g}_k = g_k V_k^\wedge,\ g_k \equiv g_k(R_k, p_k), \tag{1}$$

where $V_k^\wedge \in \mathfrak{se}(3)$ is the body-referenced Lie algebra. The *Euler-Poincaré* equation is written using $\mathfrak{se}(3) \cong \mathbb{R}^6$ as,

$$\text{Dynamics}\Big\{\ M_k\dot{V}_k + (-\mathrm{ad}_{V_k}^\top M_k)V_k = F_k\ , \tag{2}$$

where $F_k \in \mathbb{R}^6 \cong \mathfrak{se}(3)^*$ is the body wrench, and $M_k \in \mathbb{R}^{6\times 6}$ is the rigid-body inertia (see Appendix A2). In (2), $\mathrm{ad}_{V_k}^\top M_k$ encapsulates the $\mathrm{SE}(3)$ structural coefficients, and will also appear later in the context of FRS dynamics. Firstly, note that it does not satisfy skew-symmetry, see (60) in Appendix A2. This property is required in Lyapunov-based stability analysis for motion control applications [17], [24], [25], as explained in Appendix B1. Secondly, given $v, w \in \mathbb{R}^6$, the bivariate map $(\mathrm{ad}_v^\top M_k)w$ is not commutative, i.e., $(\mathrm{ad}_v^\top M_k)w \neq (\mathrm{ad}_w^\top M_k)v$, due to the non-abelian property of $\mathrm{SE}(3)$. To this end, the operator, $\mathrm{ad}_{(\bullet)}^{\sim} : \mathfrak{se}(3) \to \mathfrak{se}(3)^*$, is defined [25] such that,

$$(\mathrm{ad}_v^\top M_k)w = (\mathrm{ad}_{M_k w}^{\sim})v,\ \text{(see (61) in Appendix A2).} \tag{3}$$

Therefore, using the skew-symmetric operator, $\mathrm{ad}_{(\bullet)}^{\sim}$, (3) provides a means to exchange velocity arguments with the $\mathrm{ad}_{(\bullet)}^\top$ operator to compute the equivalent CC wrench.

Property 1: The rigid-body dynamics in (2) written alternatively using the property in (3) satisfies skew-symmetry, i.e., $x^\top\big(\frac{d}{dt}M_k - 2(-\mathrm{ad}_{M_k V_k}^{\sim})\big)x = 0$ for $x \in \mathbb{R}^6$. A corollary is that this property is invariant to a time-varying change of basis.

Proof: See Lemma A3 in Appendix A2. ∎

III. Dynamics of the FRS

In this section, due to the interdisciplinary nature of this paper, the relevant details of FRS dynamics descriptions from *both* communities, robot dynamics [1], [4] and geometric mechanics [6], [13], [26] are examined. The presentation is structured in order to facilitate a link between the two dynamic

[1]In the FRS, the velocity constraint is not externally imposed, but is a mathematical consequence of the conservation laws in the motion equations.

descriptions. For the sake of clarity, we consider the FRS as a single kinematic chain, which is formalized as follows.

Def. 1: A FRS is a multibody system of $n+1$ rigid links (see Fig. 1), which comprises of a movable FRS-base and an articulated mechanism with n holonomic joints. Its configuration space is $\mathcal{Q} \equiv \mathrm{SE}(3) \times \mathbb{R}^n$ with coordinates $r = (g_1, q) \in \mathcal{Q}$, where $g_1 \equiv (R_1, p_1) \in \mathrm{SE}(3)$ is the pose of the FRS-base and $q \in \mathbb{R}^n$ is the shape (joint positions) of the mechanism.

For general kinematic tree structures, the following computations will have an outer summation, as in [4]. In the text, the shape (q) and velocity dependencies of the dynamic quantities are provided in declaration and omitted later for brevity.

A. Floating-base Dynamics or Hamel's Equations

Considering potential forces (e.g. gravity) as external, the presence of the group coordinate g_1 yields a reduced Lagrangian [13, §5] with inertia, $M \in \mathbb{R}^{(6+n)\times(6+n)}$, as $l(q, V) = \frac{1}{2}\langle V, V\rangle_M$, where $V = \begin{bmatrix} V_1^\top & \dot{q}^\top \end{bmatrix}^\top$ is the configuration velocity, $V_1^\wedge = g_1^{-1}\dot{g}_1 \in \mathfrak{se}(3)$ for the FRS-base pose. The equations of motion that result from $l(q, V)$ are called the Hamel's equations in geometric mechanics [6, §. 6], [5, eq. 4,5] and is the Lagrangian equivalent of the floating-base formulation [19], [2], [4] in robot dynamics. It is written as,

$$\underbrace{\begin{bmatrix} M_b(q) & M_{bq}(q) \\ M_{bq}(q)^\top & M_q(q) \end{bmatrix}}_{M(q)} \begin{bmatrix} \dot{V}_1 \\ \ddot{q} \end{bmatrix} + C(q, V) \begin{bmatrix} V_1 \\ \dot{q} \end{bmatrix} = \underbrace{\begin{bmatrix} \mathcal{F}_1 \\ \tau \end{bmatrix}}_{F}, \quad (4)$$

where M_b, M_{bq}, M_q are the locked, coupling and manipulator inertias, respectively, $C \in \mathbb{R}^{(6+n)\times(6+n)}$ is the CC matrix, and $\mathcal{F}_1 \in \mathbb{R}^6 \cong \mathfrak{se}(3)^*$ and $\tau \in \mathbb{R}^n$ are the forces acting on the FRS-base and joints, respectively. A notable advantage of (4) is its efficient computation using the recursive Newton-Euler algorithm [27], [28]. The recursive form yields an iterative computation of M, C [19], [2], [27], which is outlined below.

Lemma 1: The matrices M, C in the motion equation, (4), are computed, e.g. see [27, eq. 18], as,

$$M = \sum_k T_k^\top \, M_k \, T_k, \quad (5)$$

$$C = \sum_k T_k^\top \left(-\mathrm{ad}_{V_k}^\top M_k \, T_k + M_k \, \dot{T}_k \right). \quad (6)$$

where $T_k = \begin{bmatrix} \mathrm{Ad}_{1k}^{-1}(q) & J_k(q) \end{bmatrix}$, and J_k is the link Jacobian relative to the FRS-base.

Proof: See Appendix B2. ∎

The partitioning in T_k can be used to further add detail to the dynamic matrices, e.g.

$$M = \begin{bmatrix} M_b & M_{bq} \\ M_{bq}^\top & M_q \end{bmatrix}, \; M_b = \sum_k \mathrm{Ad}_{1k}^{-\top} \, M_k \, \mathrm{Ad}_{1k}^{-1}, \\ M_{bq} = \sum_k \mathrm{Ad}_{1k}^{-\top} \, M_k \, J_k, \; M_q = \sum_k J_k^\top \, M_k \, J_k. \quad (7)$$

Note that the computation in Lemma 1 does not satisfy skew-symmetry, i.e., $x^\top(\dot{M} - 2C)x = 0, \; x \in \mathbb{R}^{6+n}$. This is commonly achieved by refactoring (6), see [19], [2], [27]. In this paper, Lemma 1 serves as a starting point to ease into the derivation of the main result, which satisfies skew-symmetry.

B. Reduced Euler-Lagrange Equations (REL): The Motivation

The dynamics in Sec. III-A only describe the FRS as a kinematic chain. However, the FRS is also uniquely characterized by a conservation property on its momentum (defined below).

Def. 2: The momentum map [5, App.] is a mapping, $\mathcal{J} : T\mathcal{Q} \to \mathfrak{se}(3)^*$, which is defined as $\mathcal{J} = \mathrm{Ad}_1^{-\top}\left(M_b V_1 + M_{bq}\dot{q}\right)$, and physically represents the total spatial momentum of the FRS.

Specifically, the conservation law on $\mathcal{J}$ is an outcome of Noether's theorem [13, §4.1] due to the SE(3) symmetry, i.e., invariance of $l(q, V)$ to g_1, in the FRS. The alternative dynamics description, which explicitly shows this property, is the set of *Reduced Euler-Lagrange* (REL) equations [13, §5.3]. In this paper, we develop a body formulation of the REL equations, i.e., using body velocity quantities. To this end, we define the locked velocity for the FRS as follows.

Def. 3: Locked velocity is the velocity of the instantaneous equivalent rigid FRS (locked shape), and is written as $\mu = V_1 + \mathcal{A}_l(q)\dot{q}$, where $\mathcal{A}_l = M_b^{-1}M_{bq}$ is the *dynamic-coupling* factor. It is the body velocity corresponding to the momentum map, i.e., $\mu = M_b^{-1}\,\mathrm{Ad}_1^\top \, \mathcal{J}$.

1) Robot Dynamics: In the robot dynamics community, a matrix-based form of the REL equations is obtained by applying dynamic congruent transformations to (4), as shown by [1], and is summarized in the Lemma below.

Lemma 2: Considering $\xi = \begin{bmatrix} \mu^\top & \dot{q}^\top \end{bmatrix}^\top$ as the new system velocity, which is related to the configuration velocity, V, through a transformation as $V = L(q)\xi$, $L = \begin{bmatrix} \mathbb{I}_{6,6} & -\mathcal{A}_l \\ 0_{n,6} & \mathbb{I}_{n,n} \end{bmatrix}$, the dynamics of the FRS are alternatively given as,

$$\underbrace{\begin{bmatrix} M_b(q) & 0_{6,n} \\ 0_{n,6} & \Lambda_q(q) \end{bmatrix}}_{\Lambda(q) = L^\top M L} \dot{\xi} + \underbrace{\begin{bmatrix} \Gamma_b(q,V) & \Gamma_{bq}(q,V) \\ \Gamma_{qb}(q,V) & \Gamma_q(q,V) \end{bmatrix}}_{\Gamma(q,V) = L^\top(M\dot{L} + CL)} \xi = \mathcal{F}, \quad (8)$$

where Λ, Γ are the transformed matrices of inertia and CC terms, and $\mathcal{F} = \begin{bmatrix} \mathcal{F}_1^\top & (\tau - \mathcal{A}_l^\top \mathcal{F}_1)^\top \end{bmatrix}^\top$ is the transformed covector of forces acting on the FRS.

Proof: See Appendix B3. ∎

Accordingly, the FRS-base pose, g_1, is reconstructed alternatively using $V_1 = \begin{bmatrix} \mathbb{I}_{6,6} & -\mathcal{A}_l \end{bmatrix} \xi$ as,

$$\dot{g}_1 = g_1\big(\mu - \mathcal{A}_l(q)\dot{q}\big)^\wedge. \quad (9)$$

Remark 1: In [1, eq. 15], the approach in Lemma 2 was used to obtain the dynamics of $(\mathcal{J}, \dot{q})$ instead of ξ. Due to the g_1-dependency of $\mathcal{J}$ in Def. 2, however, the shape dynamics had an *apparent* g_1-dependency [26, eq. 8], which is not physical. Although the shape dynamics in Lemma 2 (bottom row) does not have a g_1-dependency, its invariance to frame transformations as a property is unproved, but often assumed.

Remark 2: In (8), Γ is a placeholder CC matrix, and does not provide a special structure like the block-diagonal inertia, Λ. In particular, there is no clear separation of velocity dependencies, i.e., $\mu, \dot{q}$, in the partitions of Γ. This limits specific applications, e.g. model-based control [22], and dynamics linearization, like $\frac{\partial(\Gamma V)}{\partial \mu}$, $\frac{\partial(\Gamma V)}{\partial \dot{q}}$, which require the partitioned CC terms, preferably with closed form computation.

It is worth appreciating that the analytic form of the REL equations was revealed by the geometric mechanics community [6], [13], [26]. In this structure, notable aspects of the CC terms are velocity dependency separation and the apparentness of the curvature term. Therefore, we will subsequently review the concepts from geometric mechanics that lead to the analytic form of the REL equations. Juxtaposing it with robot dynamics in (8) will pave the way for the main result.

2) Geometric Mechanics: The conservation of $\mathcal{J}$ is written as a Pfaffian-like velocity constraint using a geometric quantity called the *mechanical connection* [7, §3.2], defined below.

Def. 4: Mechanical connection: A map, $\mathcal{A}: T\mathcal{Q} \to \mathfrak{se}(3)$, which quantifies the spatial velocity corresponding to $\mathcal{J}$, and is written as $\mathcal{A} = (M_b^s)^{-1}\mathcal{J}$, where $M_b^s = \mathrm{Ad}_{g_1^{-1}}^{\top} M_b \,\mathrm{Ad}_{g_1^{-1}}$ is the spatial locked inertia [13, eq. 5.3.1]. Using Def. 2,

$$(\mathrm{Ad}_1^{-\top} M_b \,\mathrm{Ad}_1^{-1})^{-1}\mathcal{J} = \underbrace{\mathrm{Ad}_1 \begin{bmatrix}\mathbb{I}_{6,6} & \mathcal{A}_l(q)\end{bmatrix}\begin{bmatrix}V_1 \\ \dot{q}\end{bmatrix}}_{\mathcal{A}(q,V)}, \tag{10}$$

and $\mathcal{A}_l$ is alternatively called the local *mechanical connection*.

Lemma 3: Given Def. 4, $\mathcal{A} = 0_6$ defines horizontal and vertical subspaces with velocities $V_h = (-\mathcal{A}_l\dot{q}, \dot{q})$ and $V_v = V - V_h = (V_1 + \mathcal{A}_l\dot{q}, 0_n)$, respectively, which are minimally written using the shape and locked velocities, i.e., $\dot{q}$ and μ, respectively. Using these minimal velocity forms in the orthogonal subspaces, Lemma 3 provides a geometric interpretation of the map $V = L\xi = V_v + V_h$ in Lemma 2.

Curvature of FRS: A unique characteristic of the FRS is that $\mathcal{A}$ is not preserved over a closed path in shape space, i.e., gait. In fact, this is observed through a net displacement of the FRS-base pose g_1 due to the gait, as shown in Fig. 2. This is the falling-cat phenomenon [6]. Due to its g_1-dependency, $\mathcal{A}$ in (10) is not preserved over a gait, and the amount of non-preservation is quantified by its curvature. Based on the q-dependency, just as $\mathcal{A}$ is defined locally by $\mathcal{A}_l$, the curvature of $\mathcal{A}$ is defined by the local curvature of $\mathcal{A}_l$ [13, Def. 3.5], denoted as $D\mathcal{A}_l$, where D is the exterior covariant derivative operator, see [9, §B.6]. The local curvature, $D\mathcal{A}_l$, is significant because it appears explicitly in the REL equations, as we shall see later, and is also employed for locomotion analysis in geometric mechanics [9], [10], [11], as described below.

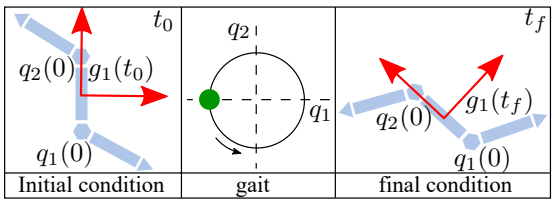

Fig. 2. Net displacement of the FRS-base, $\delta g_1 = g_1(t_0)^{-1}g_1(t_f)$, due to a gait. Left: FRS initial (t_0) configuration; Center: gait with starting point (green) and direction (arrow); Right: FRS final (t_f) configuration.

In particular, $D\mathcal{A}_l$ is exploited to estimate the net displacement of the FRS-base over a gait, i.e., $\delta g_1 = g_1(t_0)^{-1}g_1(t_f)$ in Fig. 2. Common approaches presuppose that the time-integral in (9), for $\mu = 0_6$, is converted into an area integral by invoking Stokes' theorem, see Appendix C1. In short, given an infinitesimal path displacement in shape space, $dq \in \mathbb{R}^n$, $(-\mathcal{A}_l dq)^\wedge$ in (9) defines a $\mathfrak{se}(3)$ infinitesimal displacement of the FRS-base, $\{1\}$. Similarly, for an infinitesimal *area* displacement over a gait in shape space $dA \in \mathbb{R}^n \times \mathbb{R}^n$, $(-D\mathcal{A}_l dA)^\wedge$ also quantifies a net displacement. Note that the area dA requires two base vectors to be uniquely determined.

Def. 5: The local curvature, $D\mathcal{A}_l$, in a matrix notation is $(D\mathcal{A}_l)(q,x)y = (d\mathcal{A}_l)(q,x)y - \mathrm{ad}_{\mathcal{A}_l x}\mathcal{A}_l y$, where $x, y \in \mathbb{R}^n$ are the two vectors in shape space that uniquely define the basis for an oriented differential area in the shape. The term $d\mathcal{A}_l(x)y$ is the exterior derivative operator and measures the intrinsic change in $\mathcal{A}_l$ across the shape space; and $\mathrm{ad}_{\mathcal{A}_l x}\mathcal{A}_l y$ is the Lie bracket, which measures the extrinsic change in $\mathcal{A}_l$, as the allowable velocity space rotates with the body frame, $\{1\}$, due to the non-abelian property of SE(3) [9].

Since SE(3) is non-abelian, an exact solution for δg_1 in Fig. 2 is not feasible for the FRS. However, an approximate $\delta\hat{g}_1$ over a gait area $\mathcal{U}$ is estimated as [9],

$$\zeta = \log\left(\delta\hat{g}_1\right) = -\int\int_{\mathcal{U}} D\mathcal{A}_l dA \approx \log\left(\delta g_1\right), \tag{11}$$

using visual tools to compute the area integral in (11), see Appendix C2. The approximation errors in (11) are mitigated by computing the area integral therein in the minimum perturbation coordinate frame, which minimizes non-commutativity, instead of $\{1\}$, see [8], [9]. In [11], an alternative approximation of (9) was used. In such locomotion approaches, $D\mathcal{A}_l$ is essential, and is traditionally computed using symbolic or numeric methods. A supplementary goal in this paper is to derive an analytical computation of $D\mathcal{A}_l$ using iterative robot dynamics. To facilitate a comparison with the robot dynamics notation in (8), the *unforced* matrix-based REL equations from geometric mechanics are derived next.

Lemma 4: For the *unforced* FRS, a decoupled Lagrangian, $\hat{l}(q,\xi) = \frac{1}{2}\langle\dot{q},\dot{q}\rangle_{\Lambda_q} + \frac{1}{2}\langle\mu,\mu\rangle_{M_b}$, results in the REL equations [13, §5.3], which, in matrix-based notation [26], [29] read as,

$$M_b\dot{\mu} + \frac{dM_b}{dt}\mu = \mathrm{ad}_\mu^{\top} M_b\mu - \mathrm{ad}_{\mathcal{A}_l\dot{q}}^{\top} M_b\mu, \tag{12}$$

$$\begin{aligned}\Lambda_q\ddot{q} + \frac{d\Lambda_q}{dt}\dot{q} - \frac{\partial}{2\partial q}\langle\dot{q},\dot{q}\rangle_{\Lambda_q} &= \tilde{N}(q,\mu,\dot{q}) \\ &= -\big((D\mathcal{A}_l)(\dot{q})\big)^{\top} M_b\mu + \frac{\partial\langle\mu,\mu\rangle_{M_b}}{2\partial q} - \mathcal{A}_l^{\top}\mathrm{ad}_\mu^{\top} M_b\mu.\end{aligned} \tag{13}$$

Proof: The Euler-Poincaré part is (12), and is derived in Appendix D1. In (13), the L.H.S is the Euler-Lagrange part of the shape dynamics, while $\tilde{N}$ collects the μ-dependent terms. Its expanded form is proved in Appendix D2. ■

In Lemma 4, the *unforced* case of the full FRS dynamics is interpreted as the momentum dynamics in body basis, (12), which defines the level-set on which the shape dynamics, (13), evolve. Lemma 4 further highlights the following aspects of the CC terms. Firstly, there is not only an elegant separation of the CC couplings in terms of velocity dependencies, i.e., $(\dot{q},\dot{q})$ on L.H.S and $(\dot{q},\mu),(\mu,\mu)$ on R.H.S, but they also have physical interpretations. Secondly, note that the curvature appears explicitly in (13). This structure is in contrast to (8), see Remark 2. However, (12) and (13) do not satisfy the skew-symmetric property, which is desirable, see Appendix B1.

Hence, the main idea in this paper is to modify the iterative computations from the previous works in robot dynamics [1], [19] to directly obtain the forced dynamics in (8), and separate the CC couplings as in geometric mechanics (Lemma 4). Instead of the original form of the REL equations, we derive a reformulation, which provides a skew-symmetric property.

IV. Main Contribution

In this section, the proposed form of the REL equations and its properties are derived. To ease the subsequent derivation, firstly, a direct computation is chosen to obtain (8) and avoid the transformation in Lemma 2. Secondly, the variations of the locked inertia are expressed as fundamental matrices so that they can be used in the resulting CC matrix factorization.

A. Choice of Iterative Computation

The following Lemma is stated for a general multibody system to summarize two approaches for the computation of the motion equations, while using a velocity description that is different from its configuration velocity.

Lemma 5: Given an m-DoF multibody system with configuration $r \in \mathbb{R}^m$ and configuration velocity, $\nu \in \mathbb{R}^m$, each link satisfies (2) with, $V_k = T_k(r)\nu$. An alternative system velocity $\hat{\nu} = L(r)\nu \in \mathbb{R}^m$ can be defined using a map, L. In this case, apart from the dynamics of ν, the dynamics of $\hat{\nu}$ also describes the system's motion, and can be obtained in two ways.

1) ν-Iteration+$\hat{\nu}$-Transformation: $\forall k$, $\dot{V}_k = T_k\dot{\nu} + \dot{T}_k\nu$ is substituted in (2), and pre-multiplied with $T_k^\top$ on both sides, resulting in the dynamics of the configuration velocity, ν, as in Lemma 1. Following this, $\dot{\hat{\nu}} = L\dot{\nu} + \dot{L}\nu$ is substituted in $\dot{\nu}$ from the previous result, as in Lemma 2.

2) Direct $\hat{\nu}$-Iteration: $\forall k$, V_k is rewritten as a map of the new velocity, $\hat{\nu}$, as $V_k = \tilde{T}_k(r)\hat{\nu} \Rightarrow \dot{V}_k = \tilde{T}_k\dot{\hat{\nu}} + \dot{\tilde{T}}_k\hat{\nu}$. Substituting R.H.S in (2), and pre-multiplying $\tilde{T}_k^\top$ yields the result.

Both approaches in Lemma 5 yield the same motion equations, and hence, the same inertia and CC matrix (see [20, Rem. 6]). However, Lemma 5-1 provides a numerical computation of the CC matrix in a way that its structure is concealed due to $\dot{L}$, which might be difficult to obtain in closed form. This computation was used for the FRS ($\hat{\nu} = \xi$) by [1], see Lemma 2. In contrast, Lemma 5-2 directly provides a closed form computation of the CC matrix.

Remark 3: In this paper, Lemma 5-2 shall be exploited as the first step in the derivation of the main result for the FRS ($\hat{\nu} = \xi$). To this end, the decomposition of V into velocities in the vertical and horizontal subspaces from Lemma 3 is exploited to redefine the link velocity, V_k, from Lemma 1 as, $V_k = T_k(V_v + V_h)$, which is written as,

$$V_k = \tilde{T}_k(q)\xi,\ \tilde{T}_k(q) = \begin{bmatrix}\mathrm{Ad}_{1k}^{-1}(q) & \tilde{J}_k(q)\end{bmatrix}, \qquad (14)$$

where $\tilde{J}_k = J_k - \mathrm{Ad}_{1k}^{-1}\mathcal{A}_l$ is the generalized Jacobian [1] for the k^{th} link.

B. Fundamental Matrices: Variation of Locked Inertia, M_b

For fixed-base robots, the CC matrix was shown as the sum of variations of the inertia matrix relative to time and shape [21]. These two variations were expressed as fundamental matrices (operators) that described the CC terms in the Euler-Lagrange equations. For the FRS case, we extend the notion of the fundamental matrices to describe the CC terms that arise from the variations of the locked inertia, M_b, in the REL equations of the FRS, i.e., (12)-(13). To this end, we define three operators in the respective Lemmas below.

Lemma 6: The Locked Inertia Velocity (LIV) matrix is a *symmetric* matrix, $P(q, x)$, given an arbitrary shape velocity, $x \in \mathbb{R}^n$, which is interpreted as $P(\dot{q}) = \frac{dM_b}{dt}$ when $x = \dot{q}$, and appears in (12). It is computed as,

$$P(\dot{q}) = -\sum_k \mathrm{Ad}_{1k}^{-\top}\left(\mathrm{ad}_{J_k\dot{q}}^\top M_k + M_k\mathrm{ad}_{J_k\dot{q}}\right)\mathrm{Ad}_{1k}^{-1}. \qquad (15)$$

Proof: Computing $\frac{d}{dt}M_b(q)$ using M_b in (7) and the time-derivative of the Ad operator (see Prop. 8, Appendix A), the expression of the LIV matrix, $P(q, \dot{q})$, is obtained as (15). ■

Lemma 7: Given arbitrary velocities $x, y \in \mathbb{R}^6 \cong \mathfrak{se}(3)$, the partial derivative of the scalar product $\langle x, y\rangle_{M_b}$ relative to shape (q) is written in matrix-based notation using the Locked Inertia Derivative (LID) matrix, $S(q, x)^\top$, as $\frac{\partial\langle x,y\rangle_{M_b}}{\partial q} = S(q, x)^\top y$. In the context of (13), the LID matrix is required to define the partial derivative of the locked kinetic energy relative to shape as $\frac{\partial\langle \mu,\mu\rangle_{M_b}}{\partial q} = S(q, \mu)^\top\mu$, where,

$$S(\mu)^\top = \sum_k J_k^\top\left(\mathrm{ad}^\top_{\mathrm{Ad}_{1k}^{-1}\mu}M_k + \mathrm{ad}^\sim_{M_k\mathrm{Ad}_{1k}^{-1}\mu}\right)\mathrm{Ad}_{1k}^{-1}. \qquad (16)$$

Proof: Given arbitrary x, y, the closed form computation of $S(q, x)^\top y$ is derived in Lemma 14 of the Appendix E. The expression in (16) follows as a corollary of Lemma 14 for the specific case of the locked velocity, i.e. $x = y = \mu$. ■

In the SE(3) group, the time-derivative of a covector in the body frame has an $\mathrm{ad}^\top$-term (apparent wrench) to account for changing body basis and encapsulates the SE(3) structural coefficients, as shown in Prop. 9 of Appendix A. For the FRS, the body frame is the moving FRS-base frame, $\{1\}$, which has a body velocity V_1 that depends on the shape velocity due to the *mechanical connection*, i.e., $V_1 = \mu - \mathcal{A}_l\dot{q}$. Hence, there is an additional term that accounts for the changing body basis in SE(3) due to the local *mechanical connection* through $\mathcal{A}_l\dot{q}$. This is captured by the matrix below.

Lemma 8: Given an arbitrary locked velocity $x \in \mathbb{R}^6 \cong \mathfrak{se}(3)$, and shape velocity $y \in \mathbb{R}^n$, such that $x = V_1 + \mathcal{A}_l y$, the apparent forces due to the change in the SE(3) body basis resulting from the *mechanical connection* is $\mathrm{ad}^\sim_{M_b x}\mathcal{A}_l y$, where $\mathrm{ad}^\sim_{M_b x}\mathcal{A}_l$ is the Interaction Matrix (IM) which encapsulates the product of the structure coefficients of the local *mechanical connection*, $\mathcal{A}_l$, and the SE(3) group.

Proof: The time-derivative of the locked momentum $z = M_b x$, is obtained using Prop. 9 of Appendix A2 as,

$$\frac{dz}{dt} = \mathring{z} - \mathrm{ad}_{V_1}^\top M_b x = \mathring{z} - \mathrm{ad}_x^\top M_b x + \mathrm{ad}^\top_{\mathcal{A}_l y}M_b x, \qquad (17)$$

where $\mathring{z}$ is the componentwise time-derivative (see [4, §2.10]). Note that (17) already reveals the R.H.S of (12) for $x = \mu, y = \dot{q}$. In particular, the last R.H.S term in (17) yields the apparent forces due to the change in the SE(3) body

basis resulting from the *mechanical connection*. Applying the property (3) to it as $(\mathrm{ad}^{\top}_{\mathcal{A}_l y} M_b)x = (\mathrm{ad}^{\sim}_{M_b x}\mathcal{A}_l)y$ in the spirit of the arguments of Sec. II results in the IM. ■

The REL equations are presented next with the proposed CC matrix factorization as the main contribution of this paper.

C. Proposed form of the Reduced Euler-Lagrange equations

Theorem 1: Let us consider the Floating-base Robotic System in Def. 1, given the Pfaffian-like constraint (*mechanical connection*) in Lemma 3. Its motion is governed by the *Reduced Euler-Lagrange* (REL) equations. This system of equations is proposed with the following factorization of the matrix of Coriolis/Centrifugal (CC) terms, and is written as:

$$\begin{aligned}
&\underbrace{\begin{bmatrix} M_b(q) & 0_{6,n} \\ 0_{n,6} & \Lambda_q(q) \end{bmatrix}}_{\Lambda(q)} \begin{bmatrix} \dot{\mu} \\ \ddot{q} \end{bmatrix} + \underbrace{\begin{bmatrix} \frac{1}{2}P(\dot{q}) & 0_{6,n} \\ 0_{n,6} & \tilde{\Gamma}'_q(\dot{q}) \end{bmatrix}}_{\mathcal{D}_{\dot{q}}(q,\dot{q})} \underbrace{\begin{bmatrix} \mu \\ \dot{q} \end{bmatrix}}_{\xi} \\
&= \underbrace{\begin{bmatrix} \mathrm{ad}^{\sim}_{M_b\mu} & -\frac{1}{2}S(\mu) - \mathrm{ad}^{\sim}_{M_b\mu}\mathcal{A}_l \\ \frac{1}{2}S(\mu)^{\top} - \mathcal{A}_l^{\top}\mathrm{ad}^{\sim}_{M_b\mu} & -\tilde{\mathcal{B}}(q,\mu) \end{bmatrix}}_{\mathcal{D}_{\mu}(q,\mu)} \begin{bmatrix} \mu \\ \dot{q} \end{bmatrix} \\
&+ \underbrace{\begin{bmatrix} \mathcal{F}_1 \\ \tau - \mathcal{A}_l^{\top}\mathcal{F}_1 \end{bmatrix}}_{\mathcal{F}}.
\end{aligned} \tag{18}$$

In (18), Λ is the block-diagonal inertia tensor, which is composed of the locked inertia, M_b, and the reduced shape inertia, Λ_q. The two proposed CC matrices are $\mathcal{D}_{\dot{q}}$ and $\mathcal{D}_{\mu}$, which have velocity dependencies of $\dot{q}$ and μ, respectively. These CC matrices contain the fundamental matrices defined in Lemmas 6-8. Additionally, $\tilde{\mathcal{B}}$ is related to the curvature of the local *mechanical connection*, and $\tilde{\Gamma}'$ is the reduced shape CC matrix that results in the $(\dot{q},\dot{q})$-coupling in the shape dynamics. The external forces acting on the FRS are concatenated in $\mathcal{F}$, and include the actuation and the potential (gravity) forces. In particular, given the initial conditions ($t = 0$) for $(q, \dot{q}, g_1, \mu)$, (18) is solved by computing the matrices as,

- $\Lambda_q(q) = \sum_k J_k^{\top}\, M_k\, J_k - \mathcal{A}_l^{\top}\, M_b\, \mathcal{A}_l$ (19a)
- $P(\dot{q}) = -\sum_k \mathrm{Ad}_{1k}^{-\top}\left(\mathrm{ad}^{\top}_{J_k\dot{q}} M_k + M_k \mathrm{ad}_{J_k\dot{q}}\right)\mathrm{Ad}_{1k}^{-1}$ (19b)
- $S(\mu)^{\top} = \sum_k J_k^{\top}\left(\mathrm{ad}^{\top}_{\mathrm{Ad}_{1k}^{-1}\mu} M_k + \mathrm{ad}^{\sim}_{M_k \mathrm{Ad}_{1k}^{-1}\mu}\right)\mathrm{Ad}_{1k}^{-1}$ (19c)
- $\tilde{\Gamma}'_q(\dot{q}) = \sum_k \tilde{J}_k^{\top}\left(-\mathrm{ad}^{\sim}_{M_k\tilde{J}_k\dot{q}}\,\tilde{J}_k + M_k\,\dot{\tilde{J}}_k\right)$ (19d)
- $\tilde{\mathcal{B}}(\mu) = -\mathcal{A}_l^{\top}\,\mathrm{ad}^{\sim}_{M_b\mu}\,\mathcal{A}_l + S(\mu)^T\mathcal{A}_l - \mathcal{A}_l^{\top}\,S(\mu) - \sum_k (J_k^{\top} M_k \nabla_{(\mathrm{Ad}_{1k}^{-1}\mu)} J_k)$ (19e)

where, $\tilde{J}_k = J_k - \mathrm{Ad}_{1k}^{-1}\,\mathcal{A}_l$ for the k^{th} link, and given a velocity $X \in \mathbb{R}^6 \cong \mathfrak{se}(3)$,

$$\nabla_X = M_k^{-1}(\mathrm{ad}_X^{\top} M_k + \mathrm{ad}^{\sim}_{M_k X} - M_k \mathrm{ad}_X). \tag{20}$$

Proof: A sketch of proof for Theorem 1 is shown in Fig. 3 as incremental steps that are followed here. In the following steps, the identities (68a)-(68e) from Lemma 12 related to $\tilde{J}_k$, which are listed in Appendix B, will be referred.

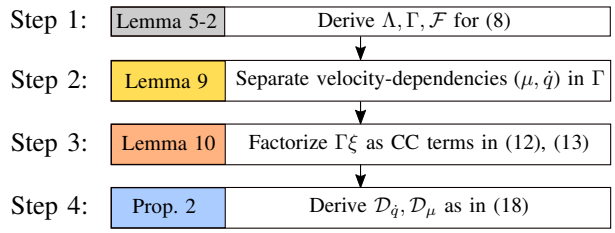

Fig. 3. A sketch of proof for Theorem 1.

Step 1: As stated in Remark 3, Lemma 5-2 is invoked with link velocity $V_k = \tilde{T}_k\xi$ to compute (8). This leads to three inferences, the first two of which corroborate the earlier results from Lemma 2, and are stated here for completeness. Firstly, the inertia matrix is obtained as, $\Lambda(q) = \sum_k \tilde{T}_k^{\top} M_k \tilde{T}_k$. Using (68a), Λ is obtained in the exact block-diagonal form of (8). Secondly, $\mathcal{F} = \sum_k \tilde{T}_k^{\top} F_k$ reduces to the same form as (8) after considering that the constraint forces in the articulated mechanism of the FRS vanish after projection.

Thirdly, the CC matrix is obtained as,

$$\Gamma(q, V_k) = \tilde{T}^{\top}\big(-\mathrm{ad}^{\top}_{V_k} M_k \tilde{T} + M_k \dot{\tilde{T}}\big). \tag{21}$$

By analysing further the closed form computation of Γ, the structure in $\mathcal{D}_{\dot{q}}, \mathcal{D}_{\mu}$ in (18) is revealed, and this is the main contribution of this paper.

Step 2: To this end, we separate the FRS velocity dependencies, i.e., μ and $\dot{q}$, in Γ. The computations are summarized in the following Lemma.

Lemma 9: The CC matrix, Γ, in (21) is obtained through the computation of its block partitions, $\Gamma_b, \Gamma_{bq}, \Gamma_{qb}, \Gamma_q$, as functions of μ and $\dot{q}$, as follows:

$$\Gamma_b = -\mathrm{ad}^{\top}_{\mu} M_b + \mathrm{ad}^{\top}_{\mathcal{A}_l\dot{q}} M_b + P(\dot{q}) \tag{22}$$

$$\Gamma_{bq} = 0_{6,n} \tag{23}$$

$$\begin{aligned}
\Gamma_{qb} =& \mathcal{A}_l^{\top}\mathrm{ad}^{\top}_{\mu} M_b - \underbrace{\sum_k J_k^{\top}\mathrm{ad}^{\top}_{\mathrm{Ad}_{1k}^{-1}\mu} M_k \mathrm{Ad}_{1k}^{-1}}_{\tilde{S}(q,\mu)^{\top}} \\
&- \underbrace{\sum_k \left(\tilde{J}_k^{\top}\mathrm{ad}^{\top}_{\tilde{J}_k\dot{q}} M_k + \tilde{J}_k^{\top} M_k\,\mathrm{ad}_{J_k\dot{q}}\right)\mathrm{Ad}_{1k}^{-1}}_{B_1(q,\dot{q})}
\end{aligned} \tag{24}$$

$$\begin{aligned}
\Gamma_q =& -\underbrace{\sum_k \tilde{J}_k^{\top}\,\mathrm{ad}^{\top}_{\mathrm{Ad}_{1k}^{-1}\mu} M_k\,\tilde{J}_k}_{B_2(q,\mu)} \\
&+ \underbrace{\sum_k \tilde{J}_k^{\top}\left(-\mathrm{ad}^{\top}_{\tilde{J}_k\dot{q}} M_k\,\tilde{J}_k + M_k\,\dot{\tilde{J}}_k\right)}_{\Gamma'_q(q,\dot{q})}.
\end{aligned} \tag{25}$$

Proof: See Appendix G1. ■

We note here that $\Gamma \neq \mathcal{D}_{\dot{q}} + \mathcal{D}_{\mu}$.

Remark 4: The last term in (22) is the LIV matrix in Lemma 6. Additionally, applying (22) and (23) to the top row of (8) results in the momentum equation of (12).

This concludes the simplification obtained through separation of dependencies in the iterative formulation. On the R.H.S of (18), we see that the $\mathcal{D}_{\mu}$ matrix only has μ-dependency

whereas Γ_{qb} in Γ from (24) has $\dot{q}$-dependency too. Also, note that in (25), $\dot{\Lambda}_q \neq \Gamma'_q + \Gamma'^{\top}_q$, which implies that the standard reduced shape space skew-symmetric property [1] for the FRS is not satisfied.

Step 3: For this, the following factorization is used to obtain the CC terms in (13) from the result in Lemma 9.

Lemma 10: Given the iterative computation of Γ in Lemma 9, the computed CC forces acting on the FRS, i.e., $\Gamma(q,\xi)\xi$ give the closed form computation of the CC forces in (12) and (13) with velocity dependencies of $\mu, \dot{q}$.

Proof: Given Γ_{qb} and Γ_q in Lemma 9, the CC torques of the shape dynamics (bottom row) in (8) are computed as,

$$\begin{aligned}\Gamma_{qb}\mu + \Gamma_q\dot{q} = &-\frac{1}{2}S(\mu)^{\top}\mu + \mathcal{A}_l^{\top}\mathrm{ad}^{\top}_{\mathcal{A}_l\dot{q}}M_b\mu \\ &+ \tilde{\mathcal{B}}(q,\mu)\dot{q} + \tilde{\Gamma}'_q(\dot{q})\dot{q},\end{aligned} \tag{26}$$

where all the CC matrices on R.H.S are the same as in Theorem 1. The proof of (26) is given in Appendix G2.

Remark 5: With the above observations, note that (26) provides the velocity dependency separation which matches the shape dynamics in (13). Also, $\tilde{\Gamma}'_q(\dot{q})\dot{q} = \big(\frac{d\Lambda_q(\dot{q})}{dt}\dot{q} - \frac{\partial\langle\dot{q},\dot{q}\rangle_{\Lambda_q}}{2\partial q}\big)$. Using the Remarks 4 and 5, we conclude that the aforementioned simplifications of the iteratively computed $\Gamma(q,\xi)\xi$ results in the CC terms of (12) and (13). ∎

However, these equations do not jointly satisfy skew-symmetry, which is often required, as noted in Appendix B1.

Step 4: Hence, we observe the following commutative property which leads to the main result in (18).

Property 2: Given locked velocities, $x, y \in \mathbb{R}^6$, and shape velocity, $z \in \mathbb{R}^n$, the following commutativity properties for the fundamental matrices from Lemmas 6 and 7 hold.

$$S(q,x)^{\top}y = S(q,y)^{\top}x,\ P(q,z)y = S(q,y)z. \tag{27}$$

Proof: For the first, $S^{\top}$ from (16) of Lemma 7 is used with (3). For the second, (3) and $\mathrm{ad}_x y = -\mathrm{ad}_y x$ are used. ∎

The Prop. 2 leads to the following corollary, which is used to obtain the result in Theorem 1.

Corollary 1: Given locked velocity $\mu \in \mathbb{R}^6 \cong \mathfrak{se}(3)^*$ and shape velocity $\dot{q} \in \mathbb{R}^n$, $P(\dot{q})\mu = \frac{1}{2}P(\dot{q})\mu + \frac{1}{2}S(\mu)\dot{q}$.

Using Corollary 1 on Γ_b in Lemma 9, followed by using (3) for both $\mathrm{ad}^{\top}$ terms, we obtain the first row in (18). Using the same property for the $\mathcal{A}_l^{\top}\mathrm{ad}^{\top}_{\mu}M_b\mu$ term in (26) provides the second row in (18). Rearranging as $(\dot{q},\dot{q})$ on L.H.S and all $(\dot{q},\mu),(\mu,\mu)$ on R.H.S, we obtain the proposed $\mathcal{D}_{\dot{q}}, \mathcal{D}_{\mu}$ matrices in (18). ∎

With Theorem 1, the CC matrix for the REL equations was obtained as a sum of two novel CC matrices, namely $\mathcal{D}_{\dot{q}}$ and $\mathcal{D}_{\mu}$. Notably, their block partitions have an explicit velocity dependency on $\dot{q}$ and μ, respectively. In contrast, the Γ matrix in (8) and the result in [1, eq. 18] have functional dependencies on V for all the block partitions instead of the velocity of the inertia-decoupling transformation, i.e., ξ. By defining the IM matrix as in Lemma 8, the same operator is used in the momentum dynamics (top) and the shape dynamics (bottom, with a transpose) of (18), in contrast to the last R.H.S term in *both*, (12) and (13). The structure of $\mathcal{D}_{\dot{q}}$ and $\mathcal{D}_{\mu}$ reveals key properties, which are provided next.

D. Key Properties of the Proposed REL Equations

1) Commutativity (Prop. 2): For fixed-base robots, we recall that the commutativity property of the CC matrix is well known [15], [21]. This property, however, does not hold for a rigid-body due to the non-abelian nature of SE(3), as discussed in Sec. II. Consequently, for the FRS, the complete CC matrix in (8) does not exhibit this property.

The separation of velocity dependencies in the CC terms of (18) enabled the isolation of the LIV matrix, P, and the LID matrix, S, for which we proved commutativity in Prop. 2. In the context of FRS dynamics, such a property has not been reported before and is neither apparent in (8) nor the pair (12)-(13). Two uses of this property are demonstrated below.

Given two velocities, $x, y \in \mathbb{R}^6$, the dynamics of the error $z = x - y$ is encountered in the stability analysis of tracking [24] and observer design [15], [25] problems. The following corollary of Prop. 2 is useful to eliminate y in such cases.

$$S(x)^{\top}x - S(y)^{\top}y = \big(2S(x)^{\top} - S(z)^{\top}\big)z. \tag{28}$$

Prop. 2 is also useful for linearization, e.g. in Kalman filtering, as is demonstrated next. Given the velocity state ξ, linearisation of the function $w = S(\mu)\dot{q}$, which appears in the top row of (18), about $\hat{\xi} = \begin{bmatrix}\hat{\mu}^{\top} & \hat{\dot{q}}^{\top}\end{bmatrix}$, gives,

$$\frac{\partial w}{\partial \xi}\Big|_{\xi=\hat{\xi}} = \begin{bmatrix}\frac{\partial w}{\partial \mu}\Big|_{\mu=\hat{\mu}} & \frac{\partial w}{\partial \dot{q}}\Big|_{\dot{q}=\hat{\dot{q}}}\end{bmatrix} = \begin{bmatrix}P(\hat{\dot{q}}) & S(\hat{\mu})\end{bmatrix} \tag{29}$$

after applying the second of Prop. 2.

2) Skew-symmetry/Passivity: This property is pivotal to energy-based analysis in control design, and is stated next.

Property 3: Given $x \in \mathbb{R}^6, y \in \mathbb{R}^n$, and $z = \begin{bmatrix}x^{\top} & y^{\top}\end{bmatrix}^{\top}$, the skew-symmetric property, $z^{\top}(\dot{\Lambda} - 2\Gamma)z = 0$, can be viewed in (18), as satisfying the following,

$$\begin{aligned}&x^{\top}\big(\frac{dM_b}{dt} - P(\dot{q})\big)x = 0,\ y^{\top}\big(\frac{d\Lambda_q}{dt} - 2\tilde{\Gamma}'_q\big)y = 0,\\ &x^{T}\mathrm{ad}^{\sim}_{M_b\mu}x = 0,\ y^{\top}\tilde{\mathcal{B}}(q,\mu)y = 0,\ z^{\top}\mathcal{D}_{\mu}z = 0.\end{aligned} \tag{30}$$

The CC matrix, $\mathcal{D}_{\dot{q}}$, which depends on $\dot{q}$, satisfies the skew-symmetry property (top row in (30)), while the CC matrix, $\mathcal{D}_{\mu}$, which depends on μ, is skew-symmetric (bottom row in (30)).

Proof: See Appendix F1. ∎

Prop. 3 is crucial for Lyapunov-based stability analysis in specific problems like motion tracking [17] and observer design [25], as explained in Appendix B1.

3) SE(3) Transformation of Momentum Dynamics: Considering an arbitrary frame as $\{C\}$, its pose $g_c(t) \in \mathrm{SE}(3)$, which may be time-varying, is a right SE(3) translation of g_1, i.e., $g_c = g_1 g_{1c}(t)$, where $\dot{g}_{1c} = g_{1c}V^{\wedge}_{1c},\ V_{1c} \in \mathfrak{se}(3)$. Correspondingly, this change of basis of μ to $\{C\}$ is an Adjoint transformation of g_{1c}, i.e., $\mu_c = \mathrm{Ad}^{-1}_{1c}\,\mu$. For this case, the following property is useful.

Property 4: The momentum dynamics (top row in (18)) transform to any time-varying frame $\{C\}$ with a pose $g_c(t) \in \mathrm{SE}(3)$ through a right SE(3) translation as,

$$\begin{aligned}\bar{M}_b(q)\dot{\mu}_c + \bar{P}(q,\dot{q},g_{1c})\mu_c = &\ \mathrm{ad}^{\sim}_{\bar{M}_b(q)\mu_c}\mu_c \\ &- \big(\frac{1}{2}\bar{S}(q,\mathrm{Ad}_{1c}\,\mu_c) + \mathrm{ad}^{\sim}_{\bar{M}_b(q)\mu_c}\bar{\mathcal{A}}_l(q,g_{1c})\big)\dot{q} + \bar{\mathcal{F}}_b,\end{aligned} \tag{31}$$

where the dynamic transformations are:

- $\bar{M}_b = \mathrm{Ad}_{1c}^{\top} M_b \mathrm{Ad}_{1c}$
- $\bar{\mathcal{A}}_l = \mathrm{Ad}_{1c}^{-1} \mathcal{A}_l$
- $\mathrm{ad}^{\sim}_{\bar{M}_b \mu_c} = \mathrm{Ad}_{1c}^{\top} \mathrm{ad}^{\sim}_{M_b \mu} \mathrm{Ad}_{1c}$
- $\bar{\mathcal{F}}_1 = \mathrm{Ad}_{1c}^{\top} \mathcal{F}_1$
- $\bar{S} = \mathrm{Ad}_{1c}^{\top} S(\mathrm{Ad}_{1c}\, \mu_c)$
- $\mathrm{ad}^{\sim}_{\bar{M}_b \mu_c} \bar{\mathcal{A}}_l = \mathrm{Ad}_{1c}^{\top} \mathrm{ad}^{\sim}_{M_b \mu} \mathcal{A}_l$
- $\bar{P} = \mathrm{Ad}_{1c}^{\top} \dfrac{P}{2} \mathrm{Ad}_{1c} + \bar{M}_b \mathrm{ad}_{V_{1c}}$

and all the L.H.S terms above have an implicit g_{1c}-dependency.

Proof: Multiplying $\mathrm{Ad}_{1c}^{\top}$ to the first row in (18), and rewriting $\mu = \mathrm{Ad}_{1c}\, \mu_c$, (31) follows. ■

Prop. 4 is useful for FRS applications that require the momentum dynamics (top row, (18)) in a more suitable frame, e.g. centroidal frame in humanoids [1], for control design and motion planning purposes.

4) $SE(3)$ Invariance of Shape Dynamics: Two key observations are made here as a corollary.

Property 5: The shape dynamics (bottom row, (18)) is invariant to the right $\mathrm{SE}(3)$ translation in Prop. 4, i.e., invariant to the transformation of the momentum dynamics like (31). Additionally, the system skew-symmetric Prop. 3 is preserved.

Proof: We note that the dynamic transformations in Prop. 4 with $\mu = \mathrm{Ad}_{1c}\, \mu_c$ satisfy,

$$\bar{\mathcal{A}}_l^{\top} \bar{M}_b \bar{\mathcal{A}}_l = \mathcal{A}_l^{\top} M_b \mathcal{A}_l,\ \bar{\mathcal{A}}_l^{\top} \bar{\mathcal{F}}_1 = \mathcal{A}_l^{\top} \mathcal{F}_1, \tag{32}$$

$$\begin{aligned} &\bar{S}(\mu_c)^{\top} \mu_c = S(\mathrm{Ad}_{1c}\, \mu_c)^{\top} \mathrm{Ad}_{1c}\, \mu_c = S(\mu)^{\top} \mu, \\ &\bar{\mathcal{A}}_l^{\top} \mathrm{ad}^{\sim}_{\bar{M}_b \mu_c} \mu_c = \mathcal{A}_l^{\top} \mathrm{ad}^{\sim}_{M_b \mu} \mu,\ \tilde{\mathcal{B}}(\mathrm{Ad}_{1c}\, \mu_c) = \tilde{\mathcal{B}}(\mu). \end{aligned} \tag{33}$$

These properties are used for the proof in Appendix F2. ■

Note that although the first in Prop. 5 appears obvious, prior works [1] have not revealed this invariance, as discussed in Remark 1. The aforementioned proof is a direct consequence of the proposed factorization of $\mathcal{D}_{\dot{q}}, \mathcal{D}_{\mu}$ in (18).

Using Properties 4 and 5, (18) is rewritten with a transformation of the proposed CC matrices as,

$$\bar{\mathcal{D}}_{\dot{q}} = \begin{bmatrix} \bar{P}(\dot{q}) & 0_{6,n} \\ 0_{n,6} & \tilde{\Gamma}'_q(\dot{q}) \end{bmatrix},$$

$$\bar{\mathcal{D}}_{\mu} = \begin{bmatrix} \mathrm{ad}^{\sim}_{\bar{M}_b \mu_c} & -\frac{\bar{S}(\mu_c)}{2} - \mathrm{ad}^{\sim}_{\bar{M}_b \mu_c} \bar{\mathcal{A}}_l \\ \frac{\bar{S}(\mu_c)^{\top}}{2} - \bar{\mathcal{A}}_l^{\top} \mathrm{ad}^{\sim}_{\bar{M}_b \mu_c} & \tilde{\mathcal{B}}(\mathrm{Ad}_{1c}\, \mu_c) \end{bmatrix}. \tag{34}$$

Applications that require the momentum in another frame (as in Prop. 4) exploit shape (joints) for control [1]. The invariance in Prop. 5 obviates the measurement of g_1 for local joint control, as we shall also demonstrate later in Sec. V.

5) Analytical Computation of Curvature: Deriving an analytical iterative computation of the local curvature for the FRS was a supplementary goal of the factorization in Theorem 1. Although symbolic forms of the FRS curvature have been proposed in geometric mechanics [16] for up to 3-shape variable systems, the iterative forms typically used in robot dynamics[2] have not been derived before. To this end, we report the following.

Theorem 2: In iterative form, the local curvature from Def. 5, $(D\mathcal{A}_l)(x)y = \big((d\mathcal{A}_l)(x) - \mathrm{ad}_{\mathcal{A}_l X} \mathcal{A}_l\big) y$, is written using the CC matrix structure in Theorem 1 as,

$$(D\mathcal{A}_l)(q,x)y = -M_b(q)^{-1} \mathcal{B}^{\top}(q,x) y,\ x, y \in \mathbb{R}^n, \tag{35}$$

[2]Note that the curvature term does not appear explicitly in the placeholder CC matrix (Γ) of (8).

where,

$$\begin{aligned} \mathcal{B}(q,x) = &\sum_k \big(J_k^{\top} (M_k \nabla_{J_k x} + 2 M_k \mathrm{ad}_{J_k x}) \mathrm{Ad}_{1k}^{-1}\big) \\ &- S(\mathcal{A}_l x)^T + \mathcal{A}_l^{\top} P(x) + \mathcal{A}_l^{\top} \mathrm{ad}^{\top}_{\mathcal{A}_l x} M_b. \end{aligned} \tag{36}$$

Proof: See Appendix F3. ■

Corollary 2: In (35), if $x = y$, $D\mathcal{A}_l = 0_6$.

Proof: See Appendix F4. ■

Property 6: (Contravariance of curvature, [13, Def. 3.5]): Given $g_c \in \mathrm{SE}(3)$ such that $g_c = g_1 g_{1c}$, the body curvature, $D\mathcal{A}_l$, transforms contravariantly to the new basis of g_c as $D\mathcal{A}_l^c = \mathrm{Ad}_{1c}^{-1} D\mathcal{A}_l$.

Proof: See Appendix F5. ■

The Prop. 6 is essential to transform Theorem 2 from the FRS-base frame, $\{1\}$, to a minimum perturbation coordinate frame (see [16], [9]), in which the approximation of Stokes's theorem on $\mathrm{SE}(3)$, (11), is optimal. Theorem 2 enables curvature computation for more than 2-shape variables, which will be demonstrated in the next section, and is useful for locomotion analysis, i.e., gait planning and initialization [8].

The key advantages of Theorem 1 over the prior results from robot dynamics (Lemma 2) and geometric mechanics (Lemma 4) are summarized in Table I through a comparison. The closed form expressions of $\mathcal{D}_{\dot{q}}, \mathcal{D}_{\mu}$ enable the linearization of the CC terms, e.g. $\frac{\partial \mathcal{D}_{\dot{q}} \xi}{\partial q}$, $\frac{\partial \mathcal{D}_{\mu} \xi}{\partial \mu}$ using existing methods, as in [19], which is not possible in Lemmas 2 and 4. Although a computational comparison merits its own scope, we provide a preliminary idea below. The computation of Γ in Lemma 2 required one pass of n iterations (link-wise), and an additional numerical transformation. The computation of $\mathcal{D}_{\dot{q}}, \mathcal{D}_{\mu}$ requires 2 passes with n iterations in each pass. One pass is nominally given by the expressions in (19), which in turn require $\mathcal{A}_l$ that is computed in a preceding pass. That being said, to emphasize this paper's contribution, the applicability of Theorem 1 and its properties is essential, and follows next.

TABLE I
COMPARISON OF FRS DYNAMICS FORMULATIONS

Property	Rob. Dyn. (Lem. 2)	Geom. Mech. (Lem. 4)	Prop. Form (Th. 1)
Commut. (Prop. 2)	✖	✖	✓
Skew-sym. (Prop. 3)	✓	✖	✓
SE(3) Transf. (Prop. 4)	✓	✓	✓
Invariance (Prop. 5)	✖	✖	✓
Curvature (Th. 2)	✖	✓	✓
CC Linearization	✖	✖	✓
Computation Complexity	Iterative n+Transform.	Symbolic –	Iterative $2n$

V. APPLICATION OF THE PROPOSED REL EQUATIONS

In this section, we emphasize the merit of Theorems 1 and 2 through practical FRS applications. In Sec. V-A, we show the benefit of the proposed CC matrix structure from Theorem 1 and its reported properties in control analysis using Lyapunov-based design. In Sec. V-B, we demonstrate the utility of Theorem 2 for curvature computation, which is required for nonholonomic locomotion analysis in geometric mechanics.

A. Output Feedback Stabilization with Non-zero Momentum

We consider the shape (joints) stabilization in the presence of non-zero momentum ($\mathcal{J} \neq 0_6$) for a gravity-free FRS, e.g. orbital robot. This control problem is relevant in orbital robotics because the FRS momentum is increased during motion synchronization with a tumbling satellite, which might have velocities up to 10[°/s]. The final robotic grasp precludes FRS-base (spacecraft) actuation ($\mathcal{F}_1 = 0_6$) from thrusters to prevent negative effects of discrete actuation. In this case, the momentum-related CC terms act as disturbance torques in the shape dynamics [14], [23]. Consequently, both works[3] showed that the standard PD-type control law results in steady-state task (position) errors. The key idea therein was to isolate the CC disturbances and compensate for them in the control law.

Here, we extend the scope of the above control problem with the practical consideration that the FRS-base velocity, V_1, is not measured. This is because the feedback of the FRS-base state, especially for the orbital robot, is often limited to only a slow-sampled (≈ 10[Hz]) and noisy pose measurement of g_1, which makes it difficult to employ numerical differentiation. We also note that this sensory limitation is relevant for other control applications that have previously assumed V_1 feedback, e.g. to reconstruct end-effector velocity [3]. To this end, in [22], we proposed an output feedback stabilization controller with an unmeasured spacecraft velocity. The available measurements of shape, q, its velocity, $\dot{q}$ and the FRS-base pose, g_1, was exploited to achieve the control task. In particular, we proposed the controller as an interconnection of an observer for the FRS states (g_1, μ) and a shape control law, which includes feed forward torques to compensate $\mu \neq 0_6$.

In this paper, we revisit this preliminary application from [22] with the aim of demonstrating the usefulness of the properties in Table I. In particular, Properties 2, 3 and 5 are used in the design. Furthermore, we use the iterative computation to show the key difference between [14] and [23], which was not done before. These aspects are remarked through the text. The estimation problem in [22] for the spacecraft states, (g_1, V_1), is summarized next.

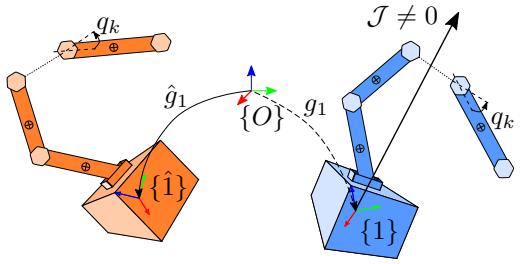

Fig. 4. Right: An orbital robot with configuration (g_1, q). Left: Its estimate with virtual configuration $(\hat{g}_1, q)$. The controller is designed to regulate the shape, while considering the available measurements, $(q, \dot{q})$, and a slow-sampled g_1 (dashed) to estimate V_1.

Let $\hat{r} = (\hat{g}_1, q) \in \mathcal{Q}$ denote the estimated configuration, where $\hat{g}_1$ is the spacecraft pose estimate of a virtual frame $\{\hat{1}\}$, see Fig. 4. The corresponding velocity of this configuration is $\hat{V} = \begin{bmatrix}\hat{V}_1^\top & \dot{q}^\top\end{bmatrix}^\top$. The configuration state estimation error, $\eta \in \mathrm{SE}(3)$ between $\hat{g}_1(t)$ and g_1, is defined[4] as $\eta(g_1, \hat{g}_1) = \hat{g}_1^{-1} g_1$. Using the log map, an error term is obtained as $\log(\eta) = \epsilon^\wedge \in \mathfrak{se}(3)$ and $\epsilon = \begin{bmatrix}\psi_1^\top & r_1^\top\end{bmatrix}^\top$, where ψ_1 and r_1 are the orientation and translational errors, respectively (see [25]). The key idea in [22] was to ensure that the state $\hat{\mu}(t) \to \mu(t)$ as $\hat{g}_1(t) \to g_1(t)$. Next, a summary of the observer from [22] is given, which is followed by the proposed shape space control laws that extend the feed forward compensation in [22].

1) SE(3) Group Observer: The kinematic part of the observer is chosen with the same geometric structure as (9) with an error injection term as follows,

$$\dot{\hat{g}}_1 = \hat{g}_1 \big(\underbrace{\hat{\mu} - \mathrm{Ad}_\eta \, \mathcal{A}_l \dot{q}}_{\hat{V}_1} + \mathrm{Ad}_\eta \, K\epsilon \big)^\wedge, \tag{37}$$

where $K : \mathbb{R}^6 \to \mathbb{R}^6$ is the observer gain which is determined through stability analysis in Sec. V-A4. In (37), note that the Ad_η operator is used to transform the body quantities from the basis of $\{1\}$ to the estimation basis of $\{\hat{1}\}$ (Fig. 4).

Error Kinematics: The observer error kinematics are derived from the time-derivative of the pose error, η, as,

$$\begin{aligned} \dot{\eta} &= -\hat{g}_1^{-1}\dot{\hat{g}}_1\hat{g}_1^{-1} g_1 + \hat{g}_1^{-1}\dot{g}_1 \\ \Rightarrow \dot{\eta} &= \eta(\mu - \mathrm{Ad}_{(\eta^{-1})}\,\hat{\mu} - K\epsilon)^\wedge \\ \Rightarrow (\eta^{-1}\dot{\eta})^\vee &= \underbrace{\mu - \mathrm{Ad}_{(\eta^{-1})}\,\hat{\mu}}_{\mu_e} - K\epsilon, \end{aligned} \tag{38}$$

where μ_e is the observer velocity error. The error kinematics, i.e., $\dot{\epsilon}$, is obtained from (38) using the *differential of exponential* from [25, Lemma 2] as,

$$\dot{\epsilon} = \mathcal{H}(\epsilon)(\eta^{-1}\dot{\eta})^\vee = \mathcal{H}(\epsilon)(\mu_e - K\epsilon), \tag{39}$$

where $\mathcal{H}(\bullet)$ is the SE(3) Jacobian, which is simply a representation Jacobian [25, Th. 2] and maps the body twist to the rate of change of the exponential coordinates, $\dot{\epsilon}$.

2) Euler-Poincaré Observer: Before describing the equations of the dynamics observer, the notion of a vector comparison between the locked velocity (μ) and the observer velocity ($\hat{\mu}$) is given. The $\mathrm{Ad}_{\eta^{-1}}$ term acts as the transport operator, which helps in defining the correct velocity error as $\mu_e = \mu - \hat{\mu}_o$, where $\hat{\mu}_o = \mathrm{Ad}_{\eta^{-1}}\,\hat{\mu}$, as is evident in (38).

Following the discussion above, the velocity error dynamics are computed by taking the time-derivative of μ_e using Prop. 8 in Appendix A and (38), as follows,

$$\begin{aligned} \frac{d}{dt}\mu_e &= \frac{d}{dt}(\mu - \mathrm{Ad}_{(\eta^{-1})}\,\hat{\mu}) \\ &= \dot{\mu} - \big(\mathrm{Ad}_{(\eta^{-1})}\,\dot{\hat{\mu}} - \mathrm{ad}_{(\mu_e - K\epsilon)}\hat{\mu}_o\big). \end{aligned} \tag{40}$$

Substituting for $\hat{\mu}_o = \mu - \mu_e$ and using the properties, $\mathrm{ad}_X X = 0_6$ and $\mathrm{ad}_X Y = -\mathrm{ad}_Y X$ in (40), we get,

$$\frac{d}{dt}\mu_e = \dot{\mu} - \big(\mathrm{Ad}_{(\eta^{-1})}\,\dot{\hat{\mu}} + \mathrm{ad}_\mu \mu_e + \mathrm{ad}_{K\epsilon}\hat{\mu}_o\big). \tag{41}$$

[3] In [14], an end-effector task was addressed, but the presented theory therein is applicable to a joint task like in [23].

[4] η is a left-invariant error [30, eq. 6], i.e., $\eta(gg_1, g\hat{g}_1) = \eta$, $g \in \mathrm{SE}(3)$.

Therefore, as in [22] , $\mathrm{Ad}_{(\eta^{-1})}\dot{\hat{\mu}}$ is determined next through an Euler-Poincaré equation, which inherits a geometric structure similar to the first row of (18) with locked velocity $\hat{\mu}_o$,

$$\begin{aligned} M_b \,\mathrm{Ad}_\eta^{-1}\,\dot{\hat{\mu}} = &-\big(\frac{1}{2}P(\dot{q}) - \mathrm{ad}^{\sim}_{M_b\hat{\mu}_o}\big)\hat{\mu}_o \\ &- \big(\frac{1}{2}S(\hat{\mu}_o) + \mathrm{ad}^{\sim}_{M_b\hat{\mu}_o}\mathcal{A}_l\big)\dot{q} + \mathcal{F}_o - M_b\mathrm{ad}_{K\epsilon}\hat{\mu}_o, \end{aligned} \tag{42}$$

where $\mathcal{F}_o \in \mathbb{R}^6 \cong \mathfrak{se}(3)^*$ is a virtual force which is determined by stability analysis in Sec. V-A4, and the last term is simply meant to cancel out the corresponding term in (41).

Velocity Error Dynamics: Substituting (42) into (41), and using the actual locked dynamics ($\dot{\mu}$) from (18), we get,

$$\begin{aligned} \frac{d}{dt}\mu_e = &M_b{}^{-1}\big(-\frac{1}{2}P(\dot{q})\mu_e - \big(\frac{1}{2}S(\mu_e) + \mathrm{ad}^{\sim}_{M_b\mu_e}\mathcal{A}_l\big)\dot{q} \\ &+ \underbrace{\big(\mathrm{ad}^{\sim}_{M_b\mu}\mu - \mathrm{ad}^{\sim}_{M_b\hat{\mu}_o}\hat{\mu}_o - M_b\mathrm{ad}_\mu\mu_e\big)}_{\tilde{\mathcal{C}}(\mu,\mu_e)\mu_e,\ \text{see Lemma 15}} - \mathcal{F}_o\big), \end{aligned} \tag{43}$$

where $\mu - \hat{\mu}_o = \mu_e$ has been used for simplification. The bracketed ad-terms can be further simplified in terms of the $\tilde{\mathcal{C}}$ operator using Lemma 15 in Appendix H. Denoting, $\Gamma_1(\dot{q},\mu,\mu_e) = -\frac{1}{2}P(\dot{q}) + \tilde{\mathcal{C}}(\mu,\mu_e)$ and $\tilde{S}(\mu_e) = -(\frac{1}{2}S(\mu_e) + \mathrm{ad}^{\sim}_{M_b\mu_e}\mathcal{A}_l)$, (43) is rewritten as,

$$\frac{d\mu_e}{dt} = M_b{}^{-1}\Big(\Gamma_1(\dot{q},\mu,\mu_e)\mu_e + \tilde{S}(\mu_e)\dot{q} - \mathcal{F}_o\Big). \tag{44}$$

Note that the velocity error dynamics in (44) is a function of the controlled quantities $\mu, \dot{q}$. Thus a separation principle between observer and controller design is not feasible since *both*, μ and $\dot{q}$ must be additionally stabilized. In the considered scenario, $\mathcal{F}_1 = 0_6$, and the manipulation task defines the control requirement. Hence, a task-based control law is proposed next to stabilize $\dot{q}$, while μ is treated as an external input.

3) Shape space Control Law: The controller consists of the observer above and additionally, a shape (joints) control law. Using the dynamics from Theorem 1, we propose a control law with two ($i = 1, 2$) alternative compensation torques, $\hat{\tau}_i \in \mathbb{R}^n$, which differ in their velocity dependency as,

$$\begin{aligned} \tau &= \tau_c + \hat{\tau}_i,\ i = 1,2 \\ \hat{\tau}_1(\hat{\mu}_o,\dot{q}) &= -(\frac{1}{2}S(\hat{\mu}_o)^\top - \mathcal{A}_l^\top\mathrm{ad}^{\sim}_{M_b\hat{\mu}_o})\hat{\mu}_o + \tilde{\mathcal{B}}(\hat{\mu}_o)\dot{q} \\ \hat{\tau}_2(\hat{\mu}_o) &= -(\frac{1}{2}S(\hat{\mu}_o)^\top - \mathcal{A}_l^\top\mathrm{ad}^{\sim}_{M_b\hat{\mu}_o})\hat{\mu}_o, \end{aligned} \tag{45}$$

where $\tau_c \in \mathbb{R}^n$ is a task controller, which is required to perform a manipulator task, and is determined through stability analysis in Sec. V-A4. The two control laws in (45) capture the results from [14] and [23], respectively, with a full-state feedback assumption, i.e., $\hat{\mu}_o = \mu, \eta = \mathbb{I}_{4,4}$.

Remark 6: The works in [14], [23] describe the FRS motion using the dynamics of $(\mathcal{J},\dot{q})$, which is obtained through the SE(3) transformation in Prop. 4. Due to the dependency of $\mathcal{J}$ on g_1 through R_1, both [14] and [23], however, report the need for attitude measurements to compute the feed forward term. Prop. 5 proved that the shape dynamics are invariant to a frame transformation for the momentum, which implies that the measurement requirement in [14], [23] arose simply from the lack of clarity in the CC terms. In fact, this measurement is avoided through the body-formulation in (45). Note that μ is simply the body velocity corresponding to $\mathcal{J}$.

Remark 7: In [14], Lemma 5-1 was used to obtain (8), which resulted in compensation torques as a function of $(\mathcal{J},\dot{q})$ because the transformation therein yielded mixed velocity dependencies in the off-diagonal terms of the CC matrix. In contrast, [23] employed a Lagrangian (Routhian) approach, which revealed compensation torques that only depend on $\mathcal{J}$. However, the CC terms were reported as partial derivatives, which lacked an iterative formulation and limits applicability to a simple FRS. By linking the iterative dynamics with the REL equations, we inherited the latter's structural benefits while extending applicability to any kinematic chain FRS. This CC matrix structure was pivotal to accommodating the control laws (using μ, not $\mathcal{J}$) from both, [14] and [23], which resulted to be different only due to the FRS dynamics formulation.

Using the control laws in (45), the shape space velocity dynamics is considered next.

Shape space Velocity Dynamics: Corresponding to i in (45), denoting $\Gamma_{q1} = \tilde{\Gamma}'_q(\dot{q}) + \tilde{\mathcal{B}}(\mu_e)$ and $\Gamma_{q2} = \tilde{\Gamma}'_q(\dot{q}) + \tilde{\mathcal{B}}(\mu)$ for ease of notation, the shape velocity dynamics are written by substituting (45) in second row of (18) as,

$$\begin{aligned} \ddot{q} = &\Lambda_q^{-1}\Big(-\Gamma_{qi}\dot{q} + \frac{1}{2}(S(\mu)^\top\mu - S(\hat{\mu}_o)^\top\hat{\mu}_o) \\ &- \mathcal{A}_l^\top\big(\mathrm{ad}^{\sim}_{M_b\mu}\mu - \mathrm{ad}^{\sim}_{M_b\hat{\mu}_o}\hat{\mu}_o\big) + \tau_c\Big). \end{aligned} \tag{46}$$

Remark 8: The corollary of Prop. 2 in (28) is crucial to simplifying the quadratic terms in (46) containing S, as,

$$S(\mu)^\top\mu - S(\hat{\mu}_o)^\top\hat{\mu}_o = \big(2S(\mu)^\top - S(\mu_e)^\top\big)\mu_e. \tag{47}$$

Additionally, using (3), followed by Lemma 15 (in Appendix H) for the $\mathcal{C}$ operator, we get,

$$\mathcal{A}_l^\top(\mathrm{ad}^{\sim}_{M_b\mu}\mu - \mathrm{ad}^{\sim}_{M_b\hat{\mu}_o}\hat{\mu}_o) = \mathcal{A}_l^\top\mathcal{C}(\mu,\mu_e)\mu_e. \tag{48}$$

Hence, substituting (28) and (48) in (46), and adding and subtracting $\mathcal{A}_l^\top\mathrm{ad}^{\sim}_{M_b\mu_e}\mu_e$ to get $\tilde{S}^\top$ from $S^\top$ (see (44)), we obtain the shape velocity dynamics as,

$$\begin{aligned} &\ddot{q} = \Lambda_q^{-1}\Big(\tau_c - \Gamma_{qi}\dot{q} + \big(\tilde{S}(\mu_e)^\top + \Gamma_2(\mu,\mu_e)\big)\mu_e\Big), \\ &\text{where, } \Gamma_2(\mu,\mu_e) = S(\mu)^\top - \mathcal{A}_l^\top(\mathcal{C}(\mu,\mu_e) + \mathrm{ad}^{\sim}_{M_b\mu_e}). \end{aligned} \tag{49}$$

Fig. 5 is the block diagram of the proposed controller (blue) with the corresponding equations for an orbital robot (orange).

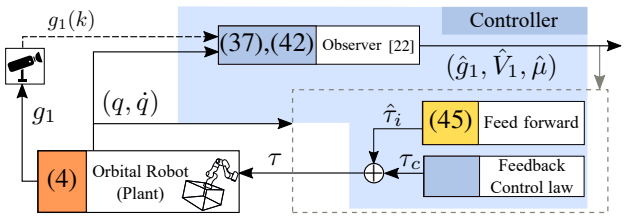

Fig. 5. A block-diagram extending the output feedback stabilization controller (blue) from [22] for an orbital robot with partial state measurements, $(g_1, q, \dot{q})$. The proposed feed forward compensation is shown in yellow.

4) Stability Analysis: Here, we prove the stability of the proposed method's error dynamics. For the task control input, τ_c, in (45), given a task set-point $q_d \in \mathbb{R}^n$, we denote $\Delta q = q - q_d$ as the task error. For the task, a positive potential function $\Phi_q(\Delta q)$ is defined with bounds as $\underline{\Phi}_q < \Phi_q < \overline{\Phi}_q$. Using its differential $d\Phi_q$, its time-derivative is written as $\dot{\Phi}_q = d\Phi_q^\top \dot{q}$. Furthermore, the error dynamics is compactly written using (39), (44) and (49) as,

$$\dot{x} = A(x,\mu)x + G(q)u, \tag{50}$$

where $x = \begin{bmatrix}\epsilon^\top & \mu_e^\top & \dot{q}^\top & \Delta q^\top\end{bmatrix}^\top$, $u = \begin{bmatrix}\mathcal{F}_o^\top & \tau_c^\top\end{bmatrix}^\top$ and

$$G^\top = \begin{bmatrix} 0_{6,6} & -{M_b}^{-1} & 0_{n,6} & 0_{n,6} \\ 0_{6,n} & 0_{6,n} & \Lambda_q^{-1} & 0_{n,n} \end{bmatrix},$$

$$A = \begin{bmatrix} -\mathcal{H}K & \mathcal{H} & 0_{6,n} & 0_{6,n} \\ 0_{6,6} & {M_b}^{-1}\Gamma_1 & {M_b}^{-1}\tilde{S} & 0_{6,n} \\ 0_{n,6} & \Lambda_q^{-1}(\tilde{S}^\top + \Gamma_2) & -\Lambda_q^{-1}\Gamma_{qi} & 0_{n,n} \\ 0_{n,6} & 0_{n,6} & \mathbb{I}_{n,n} & 0_{n,n} \end{bmatrix}.$$

Hence, the control problem is reduced to choosing u such that the error dynamics in (50) converges. Note that (50) is a non-autonomous system due to the external dependency, μ. Furthermore, A reduces to the corresponding matrix from [22] for the special case $i = 2$ in (45).

Lemma 11: For an orbital robot, defined by (4) or (18), an output feedback stabilization controller consisting of

1) SE(3) group observer defined as (37) with an error function $\eta = \hat{g}_1^{-1} g_1$ such that $\text{tr}(\eta(0)) \neq -1$,
2) an Euler-Poincaré observer as (42),
3) a shape space control law as (45), $\tau = \tau_c + \hat{\tau}_i,\ i = 1, 2$,

such that the input variable u in (50) is chosen using,

$$\mathcal{F}_o = k\mathcal{H}^\top \epsilon + P(\dot{q})\hat{\mu}_o + \text{ad}^\top_{\mathcal{A}_l \dot{q}} M_b \hat{\mu}_o + M_b \text{ad}_{\mathcal{A}_l \dot{q}} \hat{\mu}_o \tag{51}$$

$$\tau_c = -d\Phi_q(\Delta q) - D_q \dot{q} \tag{52}$$

with the observer parameter $k > 0$, task potential $\Phi_q(\Delta q)$ and damping gain, $D_q \succ 0$, the closed-loop error dynamics in (50) ensures uniform asymptotic stability of the state, x.

Proof: To use Lyapunov's direct method, the Lyapunov candidate is chosen, as in [22], as,

$$W = \underbrace{\frac{1}{2}\langle \epsilon, \epsilon \rangle_K}_{W1} + \underbrace{\frac{1}{2}\langle \mu_e, \mu_e \rangle_{M_b}}_{W2} + \underbrace{\frac{1}{2}\langle \dot{q}, \dot{q} \rangle_{\Lambda_q}}_{W3} + \Phi_q(\Delta q), \tag{53}$$

such that $K \succ 0$. We consider W for an open connected region $x(0) \in \Psi \subset \mathbb{R}^{12+2n}$, and there exist bounds as,

$$\underline{\alpha}(||x||) \leq W(x) \leq \overline{\alpha}(||x||). \tag{54}$$

Taking time-derivative along trajectories and using error dynamics in (50), we get,

$$\dot{W} = x^\top \mathcal{R} x + \dot{q}^\top(\tau_c + d\Phi_q) - \mu_e^\top \mathcal{F}_o, \tag{55}$$

where $\mathcal{R} =$

$$\begin{bmatrix} -K\mathcal{H}K & K\mathcal{H} & 0_{6,n} & 0_{6,n} \\ 0_{6,6} & (\Gamma_1 + \frac{1}{2}\dot{M}_b) & \tilde{S} & 0_{6,n} \\ 0_{n,6} & (\tilde{S}^\top + \Gamma_2) & (-\Gamma_{qi} + \frac{1}{2}\dot{\Lambda}_q) & 0_{n,n} \\ 0_{n,6} & 0_{n,6} & 0_{n,n} & 0_{n,n} \end{bmatrix}.$$

As in [22], we choose $K = k\mathbb{I}_{6,6}$ to apply the property $\mathcal{H}(\epsilon)\epsilon = \epsilon$ [25, Lemma 3] to the block matrix $(1,1)$ position.

Remark 9: The 1st in skew-symmetric Prop. 3 is pivotal to the elimination of the block matrix position $(2,2)$, while using the skew-symmetry of $\tilde{C}$ (Lemma 15) contained in Γ_1. To eliminate the block matrix $(3,3)$ position, both the 2nd and 4th of Prop. 3 are exploited. In particular, for $i = 1$ and $i = 2$, the skew-symmetry of $\tilde{\mathcal{B}}(\mu_e)$ and $\tilde{\mathcal{B}}(\mu)$, respectively, are used. Thus,

$$\begin{aligned}\dot{W} = &-k^2||\epsilon||^2 + k\epsilon^\top \mathcal{H}\mu_e + \dot{q}^\top(\Gamma_2 + 2\tilde{S}^\top)\mu_e \\ &+ \dot{q}^\top(\tau_c + d\Phi_q) + \mu_e^\top \mathcal{F}_o.\end{aligned} \tag{56}$$

Remark 10: In (56), the term $\dot{q}^\top(\Gamma_2 + 2\tilde{S}^\top)\mu_e$ is simplified due to the commutativity in Prop. 2 for S, P. For brevity, the simplifications are shown in Lemmas 16-17 in Appendix H. Following Remark 10, we obtain,

$$\begin{aligned}\dot{W} = &\mu_e^\top \Big(k\mathcal{H}^\top \epsilon - \big(P + 2\text{ad}^\top_{\mathcal{A}_l \dot{q}} M_b\big)\mu_e \\ &+ \big(P(\dot{q}) + M_b \text{ad}_{\mathcal{A}_l \dot{q}} + \text{ad}^\top_{\mathcal{A}_l \dot{q}} M_b\big)\big)\mu - \mathcal{F}_o \Big) \\ &+ \dot{q}^\top(\tau_c + d\Phi_q) - k^2||\epsilon||^2.\end{aligned} \tag{57}$$

Finally, choosing F_o, τ_c from Lemma 11, we get,

$$\dot{W} = -k^2||\epsilon||^2 - \dot{q}^\top D_q \dot{q} + \mu_e^\top \underbrace{\big(M_b \text{ad}_{\mathcal{A}_l \dot{q}} - \text{ad}^\top_{\mathcal{A}_l \dot{q}} M_b\big)}_{\text{skew-symmetric}} \mu_e$$

$$\Rightarrow \dot{W} \leq -k^2||\epsilon||^2 - \underline{\sigma}(D_q)||\dot{q}||^2 \leq 0, \tag{58}$$

which proves the uniform stability of the state x about origin. To prove asymptotic stability, the following steps are needed. Firstly, note that that $||\mu(t)|| < c_1,\ c_1 > 0$ due to the boundedness of $q, \dot{q}$ from (58) on the level-set of the momentum map, $\mathcal{J}$. Using this observation and (58), we conclude that $|\ddot{W}| < c_2$, which allows us to invoke Barbalat's Lemma and prove that $\dot{W} \to 0$, which means $||\epsilon||, ||\dot{q}|| \to 0$. Asymptotic stability follows by invoking Matrosov's theorem using the same auxiliary functions as in [22]. ■

5) Simulation: Here, we demonstrate the convergence of the controller in Lemma 11 and highlight the difference between $\hat{\tau}_1$ and $\hat{\tau}_2$. To this end, the FRS (orbital robot) consisting of the DLR's CAESAR arm [31] on the FRS-base (spacecraft) with inertia parameters from [22, §V] was considered. The observer/control parameters were chosen to provide a large settling time, as in [22, §V], and $k = l = 100$. The FRS was initialized with locked angular velocity, $\mu_\omega(0) = \begin{bmatrix}10 & 1.14 & 0\end{bmatrix}$[°/s], and the observer was initialized to the FRS state. We refer the reader to [22] for convergence and robustness results of Lemma 11 with $\hat{\tau}_2$.

In Fig. 6-**A**, the Lyapunov candidate, W (—, blue), for the proposed controller is shown to be converging, while considering $\hat{\tau}_2$. The plot of W for $\hat{\tau}_1$ is identical, and hence, not shown. This is expected because, in $\hat{\tau}_1$, $\tilde{\mathcal{B}}(\hat{\mu}_o)\dot{q}$ is a power-conserving gyroscopic torque due to the skew-symmetry (Prop. 3) of $\tilde{\mathcal{B}}$. In fact, the final position error in both cases was $||\Delta q|| \approx 0.07$[°]. However, the key difference between $\hat{\tau}_1$ and $\hat{\tau}_2$ is in the transient response, i.e., $||\dot{q}|| \neq 0$,

and is shown in Fig. 6-**B**. To emphasize this, τ_c was chosen to exhibit an underdamped response in both cases, as is evident in the shape kinetic energy, $W_3 \propto ||\dot{q}||^2$ (—, red), of Fig. 6-**A**. In Fig. 6-**B**, $||\hat{\tau}_1||$ (—, blue) shows an oscillatory behaviour due to its $\dot{q}$-dependency, whereas $||\hat{\tau}_2||$ (—, red) varies gradually with μ, and $||\hat{\tau}_1|| \to ||\hat{\tau}_2||$ as $||\dot{q}|| \to 0$. Considering the noise in $\dot{q}$ due to time-differentiation of noisy joint encoder measurements [15], $\hat{\tau}_2$ avoids noise propagation to the inner torque loop. The examination of this difference was enabled due to the computations in Theorem 1, in contrast to the motion equations used in [14] and [23].

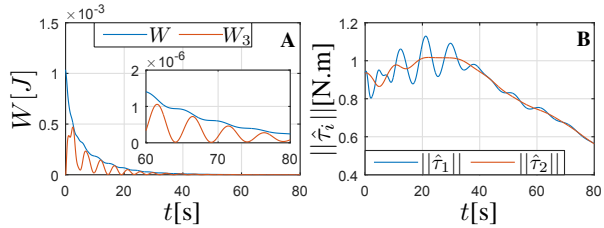

Fig. 6. **A**: Convergence, Lemma 11, **B**: Comparison between $\hat{\tau}_1$ and $\hat{\tau}_2$.

6) Discussion: The separation of velocity dependencies in the CC terms of Theorem 1 facilitated the control law in Lemma 11, which accommodated *two* compensation torque computations, see Remark 7. We additionally treated the output feedback stabilization case, and Prop. 5 obviated the requirement for g_1 measurement in the compensation (Remark 6). Commutativity in Prop. 2 was key to the analysis of error dynamics and stability, see remarks 8 and 10. The skew-symmetry in Prop. 3 was pivotal to the stability analysis (Remark 9). The result of this application was enabled only due to the aforementioned properties, which were not examined in contemporary FRS dynamics descriptions, see Table I.

B. Nonholonomic locomotion of FRS

In geometric mechanics, locomotion methods address the synthesis of a gait i.e., closed path in shape space, and its optimization to induce a desired displacement (in FRS-base) [8], [9], [10], [12], see Fig. 2. Therein, the inverse problem is commonly posed as: *Given a gait, $q(t) \in \mathbb{R}^n$, can the net FRS-base displacement, δg_1, be estimated without explicitly integrating* (9). To answer this, we refer to the well-known result from geometric mechanics [8], [9], [10] for $\mu = 0$, which, firstly, converts the integral of (9) into an area integral of curvature, as shown in Appendix C1. As a second step, a visual representation of the curvature, Constraint Curvature Function (CCF), is used to compute the resulting area integral, summarized in Appendix C2. This integral is an approximation of the FRS-base displacement per gait.

For optimal gait planning, the CCF, firstly, aids in gait synthesis, i.e., identify regions in shape space that induce negative, positive or zero displacement, for initialization and heuristics, see [12, §5]. Secondly, given a gait parameter, e.g. its perimeter, the CCF is used to solve an optimality criteria, e.g. maximize displacement and minimize perimeter [12, §6]. Recently, in [16], the idea was extended for $n > 2$ shape variables. While the aforementioned works compute the CCF map using symbolic or numeric methods for planar systems, in the following treatment, we demonstrate the application of the analytical form in Theorem 2 for a spatial FRS with $n \geq 2$, and use the CCF to answer the question posed above.

1) Motivating Scenario: To this end, let us consider the FRS in Def. 1, in which m joints (shape variables) such that $2 \leq m \leq n$ execute a gait. This gait is considered on a static embedded two-dimensional hyper-plane, $H(q) = 0$, which has local coordinates $r = \begin{bmatrix} r_1 & r_2 \end{bmatrix}^\top$ about the origin $q_c = \nabla H(q)$. Thus, there exists a unique map between the gait-space and the shape space, ψ, as,

$$q = \psi(q_c, r) \Rightarrow \dot{q} = \Psi(q_c, r)\dot{r}, \tag{59}$$

where $\Psi = \frac{\partial \psi}{\partial r} \in \mathbb{R}^{n \times 2}$ is the gait Jacobian with $n - m$ zero-rows. The concept is illustrated in Fig. 7, in which a circular gait (on a hyperplane) in an anti-clockwise sense is executed using $m = 3$ shape variables, denoted as (q_1, q_2, q_3). This scenario was considered in [32, § V.B], however, for a planar FRS with symbolically computed CCF. This motivating scenario is a typical application, in which Theorem 2 serves to generate the CCF surface map point-wise analytically.

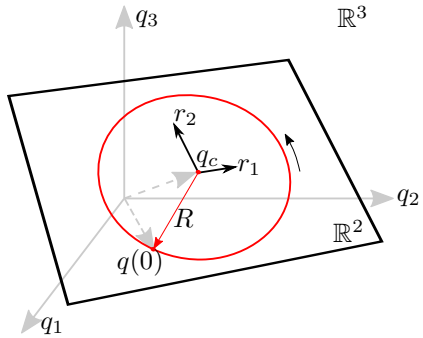

Fig. 7. A 2-Degree-of-Freedom gait-space (hyperplane) with variables (r_1, r_2) and its origin at q_c in a surrounding 3-D shape space with variables (q_1, q_2, q_3), which execute an anti-clockwise gait starting at $q(0)$.

To this end, the Algorithm 1 is the novel contribution here.

Given a gait with initial condition, $q(0)$, the following steps from [8], [9] yield an approximate FRS-base displacement.

1) Using the output of Algorithm 1, the CCF surface map is plotted over the gait-space, ϑ_r, and the CCF volume under the gait, $r(t)$, is computed to obtain the cBVI (see Appendix C2) component-wise, i.e., ζ_i in (11).
2) The net displacement in $\{C\}$, i.e., $g_c(t_0)^{-1} g_c(t_f)$ is approximated as $\exp(\zeta)$ using (11).
3) Since $g_{1c}(t_0) = g_{1c}(t_f)$ over a gait, the net displacement of the FRS-base is approximated as $\delta \hat{g}_1 = \exp(\mathrm{Ad}_{1c}\, \zeta) \approx \delta g_1$.

2) Example: For the FRS, we considered the LWR-4+ robot with $n = 7$ joints, dynamic/kinematic parameters of which were reported in [3]. The FRS-base was modeled with a mass, $m_b = 3.5$[kg] and principal inertia, $I_b \equiv (0.12, 0.14, 0.12)$[kg.m^2]. As an example, a circular gait, as in Fig. 7, was considered with $q_c = q(0) = 0_7$, and a linear gait-shape map and the gait Jacobian as $\psi = \Psi = \begin{bmatrix} 0 & 1/\sqrt{2} & 1/\sqrt{2} & 0 & 0_3 \\ 0 & 0 & 0 & 1 & 0_3 \end{bmatrix}^\top$, such that the joints

Algorithm 1 Generate CCF Surface Map

Input:

$\Psi,\ \psi,\ g_1(0),\ q_c$

Minimum perturbation coordinate (MPC) frame [8], [9], $\{C\}$, with pose $g_c \in \mathrm{SE}(3)$

Output: CCF

1: Assign basis: $e_1 = \Psi(1),\ e_2 \in \Psi(2) \in \mathbb{R}^n$, where $\Psi(i)$ is its i^{th} column
2: Compute relative pose: $g_{1c} = g_1(0)^{-1} g_c$
3: Create discretized domain (grid) of gait-space, $\vartheta_r \subset \mathbb{R}^2$ such that $r(t) \in \vartheta_r$
4: **for** each $r \in \vartheta_r$ **do**
5: Compute the configuration point in shape space: $q = \psi(q_c, r) \in \vartheta_q \subset \mathbb{R}^m$
6: Compute curvature using (35) from Theorem 2 in the FRS-base frame, $\{1\}$: $D\mathcal{A}_l(q, e_1)e_2$
7: Transform curvature to the MPC frame, $\{C\}$ using Prop. 6: $D\mathcal{A}_l^c = \mathrm{Ad}_{1c}^{-1}\, D\mathcal{A}_l$
8: CCF(index of r) $\leftarrow D\mathcal{A}_l^c$
9: **end for**
10: Save CCF to file.

numbered $2, 3, 4$, $m = 3$ are used. The circular gait was $\dot{r} = \frac{\pi}{2}\begin{bmatrix}\sin(\pi t) & \cos(\pi t)\end{bmatrix}^\top$. As in [33], the virtual chassis frame, i.e., a coordinate system located at the CoM of the FRS and oriented along its instantaneous principal axes, was chosen as the MPC frame $\{C\}$. In this frame, the locked inertia is diagonalized. Due to this choice, the translation components $k = 4, 5, 6$ can be ignored since the CoM of the FRS is invariant to shape motion, i.e., the curvature components are zero. This was also verified in the computed $\mathcal{DA}_l^c$. The Algorithm 1 from Sec. V-B1 was executed with a discrete grid size of 30×30 for ϑ_r to obtain the CCF surface data. The specific CCF surfaces are shown in Fig. 8 with the gait overlaid in blue. By visual inspection, it can be seen that the encased volumes in $k = 1, 2$ bases are small and the maximal displacement is expected along the negative $k = 3$ basis (enlarged). Indeed, upon integrating (9) with $\mu = 0_6$ and $g_1(0) = \mathbb{I}_{4,4}$, the final FRS-base orientation after the gait was found to be $(-0.4228, 0.1682, -13.73)[^\circ]$ in XYZ sense. By using the approximation in Sec. V-B1, it was found to be $(-0.9623, 0.9873, -13.25)[^\circ]$. The error metric of the pose estimate was $||\log(\delta g_1^{-1} \delta \hat{g}_1)|| = 0.017$ with an orientation error of $1.0450[^\circ]$, which is comparable to the mean error, $3.7242[^\circ]$, reported in [8]. From the similarity in the approximation error, we conclude the suitability of Theorem 2 for generating the CCF surface map using Algorithm 1 towards usage in the gait planning [8], [10], [12]. We note that the approximation method itself is not in the scope of this paper, and is used from these works here as a use-case.

The key point here is that the analytical method in Theorem 2 yields the exact curvature value at a given shape (q) in step 6 of Algorithm 1 to generate the CCF map. In contrast, numerical methods perform a numerical differentiation of $\mathcal{A}_l$ at q to obtain $D\mathcal{A}_l$, which introduces approximation errors. The advantage of the iterative computation in Theorem 2 over symbolic methods [32] is the ease of adding/removing joints seamlessly to the locomotion analysis using the same FRS model. For example, in Sec. V-B2, if the same analysis was required for joints $(1, 2, 3, 4)$, instead of the joints $(2, 3, 4)$, the symbolic computation would require a modification of the FRS model accordingly. In contrast, Theorem 2 always uses the same FRS model, and thus, offers scalability to arbitrary FRS kinematic structures, which are not restricted to be planar, i.e., $g_1 \in \mathrm{SE}(3)$. Moreover, the proposed computation provides a valid alternative to numerical and symbolic methods.

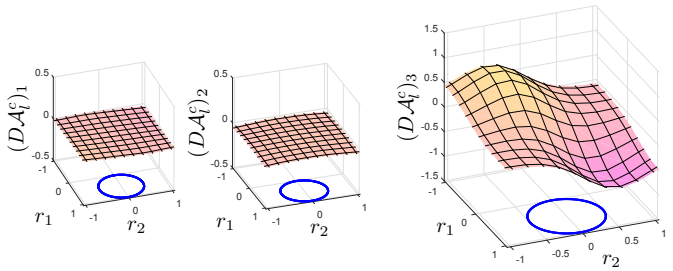

Fig. 8. CCF surface plots for the rotational bases $k = 1, 2, 3$ of the virtual chassis frame, $\{C\}$, for a 2-DoF gait (blue) using 3-shape variables.

VI. Conclusion

In this paper, we proposed a novel factorization of the Coriolis/Centrifugal (CC) matrix for the inertia-decoupled equations of a Floating-base Robotic System (FRS). The factorization was a consequence of simplifying the iteratively-computed CC matrix from robot dynamics and deriving the Reduced Euler-Lagrange (REL) equations from geometric mechanics. The proposed CC matrix is separated into two parts based on velocity dependency. The first part, which depends only on the shape velocity, was proved to satisfy the skew-symmetry (passivity) property. The second part, which depends only on the locked velocity, was proved to be skew-symmetric. We also derived novel commutative properties between two fundamental matrices that feature in the proposed CC matrices. We proved that the shape dynamics are invariant to the transformation of momentum dynamics. Using the proposed CC matrix factorization, we derived the iterative expression to compute the curvature form of the FRS. Furthermore, we demonstrated the use of the proposed CC matrix in two applications. Firstly, we derived an output feedback stabilization controller for an orbital robot, and in the stability analysis, the proposed commutative and passivity/skew-symmetric properties played a pivotal role. We also used the proposed curvature computation to estimate the FRS-base displacement due to a planar gait, while considering more than two shape variables.

Appendix

A. $SE(3)$ Group and Properties

1) Introduction: In this section, relevant details about motion on the SE(3) group are provided. The reader is referred to the Appendix A2 for the matrix descriptions of introduced quantities. The pose of a rigid-body is a matrix representation of SE(3), which is written as $g \equiv g(R, p)$, where $R \in \mathrm{SO}(3)$

is the rotation matrix and $p \in \mathbb{R}^3$ is the position. The identity of the SE(3) group is $\mathbb{I}_{4,4}$, where $\mathbb{I}_{k,k}$ is an identity matrix of dimension $k \times k$. The tangent space at $\mathbb{I}_{4,4}$ is the $\mathfrak{se}(3)$ algebra, which is referenced in body and spatial frames. Analogously, the cotangent space at $\mathbb{I}_{4,4}$ is denoted as $\mathfrak{se}(3)^*$. The $\mathfrak{se}(3)$ algebra and its dual $\mathfrak{se}(3)^*$ are isomorphic to the space of velocity twists and wrenches on $\mathbb{R}^6$ using $(\bullet)^\wedge : \mathbb{R}^6 \to \mathfrak{se}(3), \mathfrak{se}(3)^*$ and $(\bullet)^\vee : \mathfrak{se}(3), \mathfrak{se}(3)^* \to \mathbb{R}^6$, e.g. given a twist, $\mathcal{V} \in \mathbb{R}^6$, $\mathcal{V}^\wedge \in \mathfrak{se}(3)$. The adjoint action, $\mathrm{Ad} : \mathfrak{se}(3) \to \mathfrak{se}(3)$, of a pose g transforms elements of $\mathfrak{se}(3)$ algebra between spatial and body frames as $\mathcal{V}^s = \mathrm{Ad}_g \, \mathcal{V}$, see [24]. The adjoint map of the $\mathfrak{se}(3)$ algebra onto itself is $\mathrm{ad} : \mathfrak{se}(3) \to \mathfrak{se}(3)$. This is denoted by $\mathrm{ad}_\mathcal{V}$ and its coadjoint map is $\mathrm{ad}_\mathcal{V}^\top : \mathfrak{se}(3)^* \to \mathfrak{se}(3)^*$. The SE(3) group and its algebra are endowed with a diffeomorphism map, $\exp : \mathfrak{se}(3) \to \mathrm{SE}(3)$ and its inverse map, $\log : \mathrm{SE}(3) \to \mathfrak{se}(3)$ (see [25]).

2) Matrix Representation: Given a rigid-body pose $g \equiv (R, p) \in \mathrm{SE}(3)$ with body velocity $\mathcal{V} = \begin{bmatrix} \omega^\top & v^\top \end{bmatrix}^\top$ (declared in Sec. II), the following quantities are detailed,

$$\begin{aligned} g &= \begin{bmatrix} R & p \\ 0_{1,3} & 1 \end{bmatrix}, \; \mathcal{V}^\wedge = \begin{bmatrix} \omega_\times & v \\ 0_{1,3} & 0 \end{bmatrix}, \\ \mathrm{Ad}_g &= \begin{bmatrix} R & 0_{3,3} \\ p_\times R & R \end{bmatrix}, \; \mathrm{ad}_\mathcal{V} = \begin{bmatrix} \omega_\times & 0_{3,3} \\ v_\times & \omega_\times \end{bmatrix}, \end{aligned} \tag{60}$$

where $(\bullet)_\times$ is a skew-symmetric matrix for the vector, and ω (v) is the angular (linear, respectively) velocity. For k^{th}-link (see Sec. II) with mass, $m_k > 0$, the moment of inertia, $I_k \in \mathbb{R}^{3\times3} \succ 0$, and momentum $h_k = \begin{bmatrix} h_\omega^T & h_v^T \end{bmatrix}^T = M_k V_k$,

$$M_k = \begin{bmatrix} I_k & 0_{3,3} \\ 0_{3,3} & m_k \mathbb{I}_{3,3} \end{bmatrix}, \; \mathrm{ad}^\sim_{M_k V_k} = \begin{bmatrix} h_{\omega\times} & h_{v\times} \\ h_{v\times} & 0_{3,3} \end{bmatrix}. \tag{61}$$

Property 7: Corresponding to a SE(3) action of $g \in \mathrm{SE}(3)$, the following properties hold,

$$\bullet \;\; \mathrm{Ad}_g \; \mathrm{ad}_\mathcal{V} \; \mathrm{Ad}_g^{-1} = \mathrm{ad}_{\mathrm{Ad}_g \mathcal{V}} \tag{62a}$$

$$\bullet \;\; \mathrm{Ad}_g^\top \; \mathrm{ad}^\sim_{M\mathcal{V}} \; \mathrm{Ad}_g = \mathrm{ad}^\sim_{\mathrm{Ad}_g^\top M\mathcal{V}} \tag{62b}$$

Property 8: [34, Lemma 1]: Given $x \in \mathbb{R}^6$ and a pose $g \in \mathrm{SE}(3)$, which varies as $\dot{g} = gV^\wedge$ with body velocity $V \in \mathbb{R}^6 \cong \mathfrak{se}(3)$, the following holds,

$$\frac{d \, \mathrm{Ad}_g}{dt} x = \mathrm{Ad}_g \, \mathrm{ad}_V x. \tag{63}$$

Property 9: [34, Lemma 2]: Given a time-varying frame with pose $g \in \mathrm{SE}(3)$, which moves as $\dot{g} = gV^\wedge$, where $V \in \mathbb{R}^6 \cong \mathfrak{se}(3)$ is the frame body velocity, the time-derivative of a covector $y \in \mathbb{R}^6 \cong \mathfrak{se}(3)^*$ in this frame is given by,

$$\frac{d}{dt} y = \mathring{y} - \mathrm{ad}_V^\top y, \tag{64}$$

where $\mathring{y}$ is the componentwise time-derivative (see [4, §2.10]), and $\mathrm{ad}_V^\top y$ accounts for the basis change of the time-varying frame, and encapsulates the SE(3) structural coefficients.

3) Proof in Property 1: The first part follows because M_k is a constant and $\mathrm{ad}^\sim_{M_k V_k}$ is skew-symmetric. For the corollary, a time-varying frame $\{C\}$ with a pose $g_c \in \mathrm{SE}(3)$ is considered, which is a right translation of g_k, i.e., $g_c = g_k g_{kc}$, where $g_{kc} \in \mathrm{SE}(3)$ evolves as $\dot{g}_{kc} = g_{kc} V_{kc}^\wedge$. In the basis of $\{C\}$, $\bar{V}_k = \mathrm{Ad}_{kc}^{-1} V_k$, and taking its time-derivative using (2) and Prop. 7 from Appendix A leads to,

$$\bar{M}_k \dot{\bar{V}}_k + (-\mathrm{ad}^\sim_{\bar{M}_k \bar{V}_k} + \bar{M}_k \mathrm{ad}_{V_{kc}}) \bar{V}_k = \bar{F}_k, \tag{65}$$

where $\bar{M}_k = \mathrm{Ad}_{kc}^\top M_k \, \mathrm{Ad}_{kc}$ and $\bar{F}_k = \mathrm{Ad}_{kc}^\top F_k$. In (66), for $x \in \mathbb{R}^6$, $x^\top \big(\frac{d}{dt} \bar{M}_k - 2(-\mathrm{ad}^\sim_{\bar{M}_k \bar{V}_k} + \bar{M}_k \mathrm{ad}_{V_{kc}}) \big) x = 0$ is satisfied, which proves the invariance of the skew-symmetry to a change (time-varying) of basis, i.e., a frame transformation.

B. Multibody Dynamics

1) Passivity/Skew-symmetry: Given a mechanical system with velocity $V \in \mathbb{R}^m$ and inertia M, the unforced motion equations result from the kinetic energy, $\kappa = \frac{1}{2} \langle V, V \rangle_M$, as,

$$M\dot{V} + C(V)V = 0, \tag{66}$$

where CV is the CC force.

Passivity in (66), i.e., $V^\top \big(\dot{M} - 2C \big) V = 0$, is pivotal in Lyapunov stability analysis of controller designs [1], [3], in which, the time-derivative of kinetic energy, $\dot{\kappa}$ is computed. Using (66), $\dot{\kappa} = V^\top \big(\frac{\dot{M}}{2} - C \big) V$, and passivity implies $\dot{\kappa} = 0$, i.e., 0 power flow due to the CC force.

In specific control problems like tracking [17] and observer design [25], a kinetic-like energy function appears as $\hat{\kappa} = \frac{1}{2} \langle w, w \rangle_M$, where $w \in \mathbb{R}^m$ is, for example, a velocity error. In such cases, the time-derivative of $\hat{\kappa}$ contains $w^\top \big(\frac{\dot{M}}{2} - C \big) w$, which is not 0 despite passivity. Hence, a stronger skew-symmetry property is desired for the C matrix to conclude 0 power flow due to the CC wrench.

2) Proof of Lemma 1: The velocity of the k^{th} link is $V_k = T_k(q) V$ and its time-derivative is $\dot{V}_k = T_k(q) \dot{V} + \dot{T}_k(V) V$. Substituting this in (2) for all links, pre-multiplying $T_k^\top$ on both sides and considering that the constraint reaction wrenches disappear after projection results in (4) with M, C as in (5) and 6. Note that an iterative loop is required in Lemma 1, and T_k and $\dot{T}_k$ are obtained beforehand in this loop through a recursive computation, as shown in [19, §VI].

3) Proof of Lemma 2: Substituting $\dot{V} = L\dot{\xi} + \dot{L}\xi$ in (4), and multiplying $L^\top$ on the L.H.S results in (8) with Λ, Γ as numerical transformations of M, C (in underbraces of (8)).

Property 10: Given the FRS (see Fig. 1) defined in Def. 1, for $\mathcal{V} \in \mathbb{R}^6 \cong \mathfrak{se}(3)$,

$$\sum_k \mathrm{Ad}_{1k}^{-\top} \; \mathrm{ad}^\top_{\mathrm{Ad}_{1k}^{-1} \mathcal{V}} M_k \mathrm{Ad}_{1k}^{-1} = \mathrm{ad}_\mathcal{V}^\top M_b. \tag{67}$$

Proof: Using (62a) in Prop. 7 from Appendix A for simplification of L.H.S, followed by substitution of the iterative expansion of M_b from (7), we get the result. ∎

The following identities related to $\tilde{J}_k$ will be used for the proof of Theorem 1.

Lemma 12: The following identities hold true.

$$\sum_k \mathrm{Ad}_{1k}^{-\top} \; M_k \, \tilde{J}_k = 0_{6,n} \tag{68a}$$

$$\sum_k \mathrm{Ad}_{1k}^{-\top} \; M_k \, \dot{\tilde{J}}_k = \sum_k \mathrm{Ad}_{1k}^{-\top} \; \mathrm{ad}^\top_{J_k \dot{q}} \, M_k \, \tilde{J}_k \tag{68b}$$

$$\sum_k \mathrm{Ad}_{1k}^{-\top} \; \mathrm{ad}^\sim_{M_k \tilde{J}_k \dot{q}} \, \mathrm{Ad}_{1k}^{-1} = 0_{6,n} \tag{68c}$$

$$\sum_k \mathrm{Ad}_{1k}^{-\top}\, \mathrm{ad}^{\top}_{\mathrm{Ad}^{-1}_{1k}\mu}\, M_k \tilde{J}_k = 0_{6,n} \tag{68d}$$

$$\sum_k \mathrm{Ad}_{1k}^{-\top}\, \left(\mathrm{ad}^{\top}_{J_k\dot{q}} - \mathrm{ad}^{\top}_{\tilde{J}_k\dot{q}}\right)\, M_k \tilde{J}_k = 0_{6,n} \tag{68e}$$

Proof: To prove (68a), in the iteration of (7), the expression of $\tilde{J}_k$ is used instead of J_k, while all the other identities are a direct consequence of (68a), (62a) and (62b) from the Prop. 7 in Appendix A. ■

C. Application of Stokes' Theorem for the FRS

1) Stokes' Theorem: Let us assume $\mathcal{J} = 0_6 \Rightarrow \mu = 0_6$ for simplicity of exposition, which reduces (9) to

$$\dot{g}_1 = g_1(-\mathcal{A}_l\dot{q})^{\wedge}, \tag{69}$$

and that the initial condition is $g_1(0) = \mathbb{I}_{4,4}$. Under an abelian group assumption[5] for g_1, the solution for (69) is [10],

$$g_1(t_f) = \exp\Big(\int_{t_0}^{t_f} -\mathcal{A}_l\dot{q}dt\Big) = \exp\Big(\int_{\partial\mathcal{U}} -\mathcal{A}_l dq\Big), \tag{70}$$

where for $X \in \mathbb{R}^6$, $\exp(X) \equiv \exp(X^{\wedge})$ is the SE(3) exponential [24]. Note that the time-integral is replaced by a path-integral over a path $\partial\mathcal{U}$. For a closed path, i.e., gait, Stokes' theorem [10] is applied to convert the path integral in (70) to an area integral over the area $\mathcal{U}$,

$$g_1(t_f) = \exp\Big(-\int\int_{\mathcal{U}} D\mathcal{A}_l dA\Big), \tag{71}$$

where, $(D\mathcal{A}_l)(x)y = (d\mathcal{A}_l)(x)y - \mathrm{ad}_{\mathcal{A}_l x}\mathcal{A}_l y$ is a map $D\mathcal{A}_l : \mathbb{R}^n \times \mathbb{R}^n \to \mathfrak{se}(3)$ and is the local curvature, i.e., the covariant derivative of the local connection form $\mathcal{A}_l x$ along shape trajectories given by y, and dA is a differential area that is parameterized by the basis vectors $x, y \in \mathbb{R}^n$. The integral of $(d\mathcal{A}_l)(x)y$ in (71) is the nonconservative contribution and captures the change in *mechanical connection* due to change in shape. Likewise, the integral of the Lie bracket term $-\mathrm{ad}_{\mathcal{A}_l x}\mathcal{A}_l y$ is the the primary non-commutative contribution and captures the change in *mechanical connection* due to non-commutativity of SE(3) [9].

2) FRS-base Displacement over a Gait: Plotting the curvature, $D\mathcal{A}_l$, component-wise over the gait's domain produces the Constraint Curvature Function (CCF) surfaces, see Fig. 9. By computing the CCF surface volume under the gait area, we obtain the corrected Body Velocity Integral (cBVI), i.e., ζ in (11). Using this, an approximate $\delta\hat{g}_1 = \exp(\zeta)$ per gait cycle is obtained [9]. We elaborate the main idea for a 2-joint FRS (see Fig. 2), and hence the gait is defined by the shape basis vectors $(q_1, q_2) \in \mathbb{R}^2$. In Fig. 9, the CCF for the k^{th} component[6], $(D\mathcal{A}_l)_k$ is plotted on the left as a surface with an overlay of a circular gait (red). On the right of Fig. 9, the volumetric mesh of the CCF surface under the gait area (red) is shown. The positive sense (arrows) is given by the direction of gait is execution. By computing the volume of the CCF surfaces for each component (k), we obtain the corresponding component, ζ_k. Finally, $\exp(\zeta) = \delta\hat{g}_1$ is the approximation of the net displacement of the FRS-base, δg_1, over the gait.

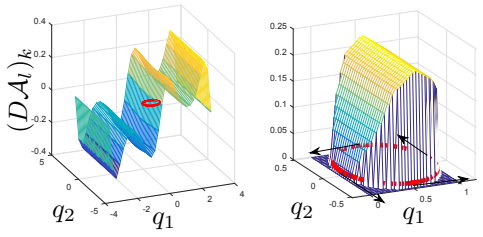

Fig. 9. CCF surface for the k^{th} basis corresponding to a gait (red circle) using 2-joints, and its zoomed in mesh volume (right) under that gait area, which provides an approximate estimate of FRS-base displacement per gait.

D. Derivations for REL Equations in Lemma 4

1) Proof of (12)*:* The momentum equation [26, eq. 6] is,

$$\langle \frac{dp}{dt}, \eta\rangle = \langle p, [(-\mathcal{A}_l\dot{q} + M_b^{-1}p)^{\wedge}, \eta^{\wedge}]^{\vee}\rangle,\ \eta \in \mathbb{R}^6. \tag{72}$$

Moving η to the left on L.H.S and R.H.S after using SE(3) Lie-bracket isomorphism, $[x^{\wedge}, y^{\wedge}]^{\vee} = \mathrm{ad}_x y,\ x, y \in \mathbb{R}^6$, substituting $p = M_b\mu$ and, eliminating η yields the result.

2) Proof of (13)*:* To obtain closed form expression for $\tilde{N}$ in (13), we recall [35, eq. 3.11.19][7], which provides a scalar product form in terms of body momentum, $p = M_b\mu$, as,

$$\begin{aligned}\langle \tilde{N}, \delta q\rangle = -\Big\langle p, (d\mathcal{A}_l)(q,\dot{q},\delta q) - [(\mathcal{A}_l\dot{q})^{\wedge}, (\mathcal{A}_l\delta q)^{\wedge}]^{\vee} \\ + \frac{1}{2}\frac{\partial(M_b{}^{-1}p)}{\partial q}\delta q + [(M_b{}^{-1}p)^{\wedge}, (\mathcal{A}_l\delta q)^{\wedge}]^{\vee}\Big\rangle.\end{aligned} \tag{73}$$

In (73), as in Appendix D1, the isomorphism, $[x^{\wedge}, y^{\wedge}]^{\vee} = \mathrm{ad}_x y$ is used. Also, in vector notation, $(d\mathcal{A}_l)(q,\dot{q},\delta q) = (d\mathcal{A}_l)(q,\dot{q})\delta q$. And, $\frac{\partial(M_b{}^{-1}p)}{\partial q} = -M_b{}^{-1}\frac{\partial M_b(M_b{}^{-1}p)}{\partial q}$. Moving all δq terms towards the left in both L.H.S and R.H.S of (73), and substituting p, we get,

$$\begin{aligned}\langle \delta q, \tilde{N}\rangle = \Big\langle \delta q, \big(-(d\mathcal{A}_l)(q,\dot{q})^{\top} - \mathcal{A}_l^{\top}\mathrm{ad}^{\top}_{\mathcal{A}_l\dot{q}}\big)M_b\mu \\ + \frac{1}{2}\frac{\partial\mu^{\top}M_b(q)\mu}{\partial q} - \mathcal{A}_l^{\top}\mathrm{ad}^{\top}_{\mu}M_b\mu\big)\Big\rangle.\end{aligned} \tag{74}$$

Removing δq variations, we get $\tilde{N}$ in (13).

E. Computation of the LID Matrix in Lemma 7

The following Lemma, which is an application of [19, Prop. 4], is key to the proof in Lemma 14.

Lemma 13: Given a column-wise detail of link Jacobian as, $J_k = \begin{bmatrix} J_k^1 & \dots & J_k^n \end{bmatrix}$ for the k^{th} link, using [19, Prop. 4] for the j^{th} joint and a velocity $X \in \mathbb{R}^6 \cong \mathfrak{se}(3)$, we have,

$$\begin{aligned}\frac{\partial \mathrm{Ad}_{1k}^{-1}X}{q_j} &= -\mathrm{ad}_{J_k^j}\mathrm{Ad}_{1k}^{-1}X \\ \Rightarrow \frac{\partial \mathrm{Ad}_{1k}^{-1}X}{\partial q} &= \begin{bmatrix} -\mathrm{ad}_{J_k^1}\mathrm{Ad}_{1k}^{-1}X & \dots \end{bmatrix}.\end{aligned} \tag{75}$$

[5]The assumption is used to explain the main idea. However, SE(3) is not an abelian group, and despite the failure of the assumption, the presented theory was shown to be an approximation of the exact solution [9], [10].

[6]In $\mathfrak{se}(3) \cong \mathbb{R}^6$, $k = 1, \dots, 6$, where the first three indices refer to the rotational and the last three to the translational bases, respectively.

[7]In [35, eq. 3.11.19], the μ-dependent terms are on the L.H.S.

Lemma 14: The partial derivative of the scalar form $\langle x, y\rangle_{M_b},\ x, y \in \mathbb{R}^6$ with respect to q is computed as,

$$\frac{\partial}{\partial q}\langle x, y\rangle_{M_b} = \sum_k \big(\Pi_k(x)^\top + \tilde{\Pi}_k(x)\big)y = S(x)^\top y, \quad (76)$$

$$\sum_k \Pi_k(x)^\top = \sum_k J_k^\top \mathrm{ad}^\top_{\mathrm{Ad}_{1k}^{-1}x} M_k \mathrm{Ad}_{1k}^{-1}, \quad (77)$$

$$\sum_k \tilde{\Pi}_k(x) = \sum_k J_k^\top \mathrm{ad}^\sim_{M_k \mathrm{Ad}_{1k}^{-1}x} \mathrm{Ad}_{1k}^{-1}. \quad (78)$$

Proof: Considering that $\mathrm{Ad}_{1k} \equiv \mathrm{Ad}_{1k}(q)$, note that,

$$\begin{aligned}\frac{\partial}{\partial q}\langle x, y\rangle_{M_b} &= \sum_k \frac{\partial}{\partial q}\Big(\big(\underbrace{\mathrm{Ad}_{1k}^{-1}x}_{r(q)}\big)^\top M_k \big(\underbrace{\mathrm{Ad}_{1k}^{-1}y}_{s(q)}\big)\Big)\\ &= \sum_k \Big(\big(\frac{\partial r(q)}{\partial q}\big)^\top M_k s(q) + \big(\frac{\partial s(q)}{\partial q}\big)^\top M_k r(q)\Big) \quad (79)\\ &= \sum_k \Pi_k(x)^\top y + \Pi_k(y)^\top x,\end{aligned}$$

where $\Pi_k(z) = \mathrm{Ad}_{1k}^{-\top} M_k \frac{\partial \mathrm{Ad}_{1k}^{-1} z}{\partial q}$. Now, we invoke Lemma 13, and apply the property, $\mathrm{ad}_{J_k^j}\mathrm{Ad}_{1k}^{-1}x = -\mathrm{ad}_{\mathrm{Ad}_{1k}^{-1}x}J_k^j$ in it. Isolating, J_k^j to obtain J_k, we first obtain $\frac{\partial \mathrm{Ad}_{1k}^{-1}x}{\partial q} = \mathrm{ad}_{\mathrm{Ad}_{1k}^{-1}x}J_k$. Substituting this in Π_k yields (77).

The result in second of (79) can be conveniently rewritten as a linear operator form as (76) such that $\Pi_k(y)^\top x = \tilde{\Pi}_k(x)y$. This velocity exchange property appears similar to the one in (3) and is actually a consequence of it. By simply exploiting the property in (3) in $\Pi_k(y)^\top x$, we obtain (78). ∎

F. Proofs about Key Properties in Sec. IV-D

1) Proof of Prop. 3: The first follows straightforwardly. The second follows by using the corresponding matrix expansions in (19a) and (19d). For the third, fourth and fifth, $\mathrm{ad}^\sim_{M_b\mu}$, $\tilde{\mathcal{B}}$ in (19e) and $\mathcal{D}_\mu$ in (18), respectively, are skew-symmetric. The final claim is evident in the velocity dependencies of $\mathcal{D}_{\dot{q}}, \mathcal{D}_\mu$.

2) Proof of Prop. 5: Using the first of (32) in (19a), we conclude that Λ_q is invariant. The second of (32) implies that the reduced joint torques, $\tau - \mathcal{A}_l^\top \mathcal{F}_1$, in (18) are also invariant. In (19d), $\tilde{\Gamma}'_q$ is invariant because its computation depends on body Jacobians, $\tilde{J}_k$, which are invariant to spatial frame transformations. Finally, substituting $\mu = \mathrm{Ad}_{1c}\,\mu_c$ in (18) and using (33), we conclude that the CC torques are invariant. Thus, the invariance of the shape dynamics in (18) to frame transformations follows. The second follows straightforwardly from Prop. 4. In particular, $x^\top(\frac{d}{dt}\bar{M}_b - 2\bar{P})x = 0$ for $x \in \mathbb{R}^6$ is the multibody equivalent of the corollary in Prop. 1.

3) Proof of Theorem 2: The iterative form of the curvature is obtained by matching (13) and the bottom row of (18). Following Remark 5, by elimination, the only remaining terms are $-\tilde{\mathcal{B}}(\mu)\dot{q}$ in (18) and $-((D\mathcal{A}_l)(q,\dot{q}))^\top M_b\mu$ in (13), which are equal[8]. Considering a generalized velocity x instead of $\dot{q}$, (19e) is reformulated as $-\tilde{\mathcal{B}}(\mu)x = \mathcal{B}(q,x)\mu$ to obtain the new matrix operator in (36). This reformulation of $-\tilde{\mathcal{B}}(\mu)x$ is performed by applying the properties $\mathrm{ad}_X Y = -\mathrm{ad}_Y X$, (3), and the proposed Prop. 2. Hence, by equating, $-\tilde{\mathcal{B}}(\mu)x = \mathcal{B}(x)\mu = -((D\mathcal{A}_l)(q,x))^\top M_b\mu$, we get the result in Theorem 2. In particular, we further isolate the exterior derivative operator as,

$$\begin{aligned}(d\mathcal{A}_l)(x)y = -M_b^{-1}\Big(&- S(\mathcal{A}_l x) + P(x)\mathcal{A}_l\\ &+ \sum_k \big(J_k^\top(M_k\nabla_{J_k X} + 2M_k\mathrm{ad}_{J_k x})\mathrm{Ad}_{1k}^{-1}\big)^\top\Big).\end{aligned} \quad (80)$$

4) Proof of Corollary 2: Substituting $x = y$, the final term in $\mathcal{B}^T$ cancels out because $\mathrm{ad}_X X = 0$. Applying Prop. 2, the two middle terms cancel each other. In the first term, using (20), all the terms cancel out and yield the result.

5) Proof of Prop. 6: The transformed curvature, $D\mathcal{A}_l^c$, is obtained using (35), but with the matrices $M_b, \mathcal{B}$ referred in the basis of g_c, i.e., $\hat{M}_b = \mathrm{Ad}_{1c}^\top M_b\,\mathrm{Ad}_{1c}$ and[9] $\mathcal{B}_c(q,x) = \mathcal{B}(q,x)\,\mathrm{Ad}_{1c}$, as $D\mathcal{A}_l^c = \hat{M}_b^{-1}\mathcal{B}_c(x)^\top$. Substituting the constituent matrices yields the result.

G. Proofs used in Theorem 1 (Main Result)

1) Proof of Lemma 9: The partitions of the CC matrix, Γ, in (21) are expanded by using partitions of $\tilde{T}$ from (14) of Remark 3. The main idea of this proof is to start from these expressions and separate the terms according to their velocity dependencies for each of the four blocks of Γ in (21). In fact, the key feature of the CC matrix structure in (18) is the isolation of different terms according to the dependency on shape ($\dot{q}$) and locked (μ) velocities. This step will also reveal the LIV matrix structure defined above in (15).

Expanding the CC matrix, Γ, using (14) yields

$$\Gamma_b = \sum_k \mathrm{Ad}_{1k}^{-\top}\left(-\mathrm{ad}^\top_{V_k}M_k - M_k\,\mathrm{ad}_{J_k\dot{q}}\right)\mathrm{Ad}_{1k}^{-1} \quad (81a)$$

$$\begin{aligned}\Gamma_{bq} &= \sum_k \mathrm{Ad}_{1k}^{-\top}\left(-\mathrm{ad}^\top_{V_k}M_k\tilde{J}_k + M_k\,\dot{\tilde{J}}_k\right)\\ &= \sum_k \mathrm{Ad}_{1k}^{-\top}\left(-\mathrm{ad}^\top_{V_k}M_k + \mathrm{ad}^\top_{J_k\dot{q}}M_k\right)\tilde{J}_k\end{aligned} \quad (81b)$$

$$\Gamma_{qb} = \sum_k \tilde{J}_k^\top\left(-\mathrm{ad}^\top_{V_k}M_k - M_k\,\mathrm{ad}_{J_k\dot{q}}\right)\mathrm{Ad}_{1k}^{-1} \quad (81c)$$

$$\Gamma_q = \sum_k \tilde{J}_k^\top\left(-\mathrm{ad}^\top_{V_k}M_k\tilde{J}_k + M_k\,\dot{\tilde{J}}_k\right), \quad (81d)$$

where (68b) is used to get (81b). For the proof, Γ is factorized into $(\dot{q},\dot{q})$, $(\dot{q},\mu)$ and (μ,μ) couplings. The key idea is to use (14) to write $V_k = \mathrm{Ad}_{1k}^{-1}\mu + \tilde{J}_k\dot{q}$ and split $\mathrm{ad}^\top_{V_k}M_k$ in (81) as the sum of contributions depending on $\dot{q}$ and μ, as,

$$\mathrm{ad}^\top_{V_k}M_k = (\mathrm{ad}^\top_{\mathrm{Ad}_{1k}^{-1}\mu} + \mathrm{ad}^\top_{\tilde{J}_k\dot{q}})M_k. \quad (82)$$

- Γ_b in (22): We simplify (81a) by splitting $\mathrm{ad}^\top_{V_k}$ as,

$$\begin{aligned}\Gamma_b = \sum_k \mathrm{Ad}_{1k}^{-\top}\Big(&- \big(\mathrm{ad}^\top_{\mathrm{Ad}_{1k}^{-1}(\mu - \mathcal{A}_l\dot{q})} + \mathrm{ad}^\top_{J_k\dot{q}}\big)M_k\\ &- M_k\,\mathrm{ad}_{J_k\dot{q}}\Big)\mathrm{Ad}_{1k}^{-1}\end{aligned} \quad (83)$$

[8] This observation has also been remarked in [29, §4]

[9] In the new basis, $\mu_c = \mathrm{Ad}_{1c}^{-1}\,\mu$, which is substituted in $\mathcal{B}$ to get $\mathcal{B}_c$.

The summation in (83) is eliminated after using the expansion for $P(\dot{q})$ from (15), and applying Prop. 10 (Appendix B). This yields (22) in Lemma 9.

- Γ_{bq} in (23): After expanding $\tilde{J}_k$ in (81b), we obtain,

$$\begin{aligned}\Gamma_{bq} &= \sum_k \mathrm{Ad}_{1k}^{-\top}\big(\mathrm{ad}^{\top}_{(-\mathrm{Ad}_{1k}^{-1}\mu-\tilde{J}_k\dot{q}+J_k\dot{q})}M_k\big)\tilde{J}_k \\ &= -\sum_k \mathrm{Ad}_{1k}^{-\top}\left(\mathrm{ad}^{\top}_{\mathrm{Ad}_{1k}^{-1}\mu}+\mathrm{ad}^{\top}_{(\tilde{J}_k\dot{q}-J_k\dot{q})}\right)M_k\,\tilde{J}_k\end{aligned} \tag{84}$$

Using Prop. 10 (Appendix B) and applying (68d) and (68e) straightforwardly yields (23).

- Γ_{qb} in (24): Using (82) and the form of $\tilde{J}_k$ from (14) to expand the terms in (81c), we get,

$$\begin{aligned}\Gamma_{qb} &= \sum_k \tilde{J}_k^{\top}\big(-\mathrm{ad}^{\top}_{(\mathrm{Ad}_{1k}^{-1}\mu+\tilde{J}_k\dot{q})}M_k - M_k\,\mathrm{ad}_{J_k\dot{q}}\big)\mathrm{Ad}_{1k}^{-1} \\ &= \sum_k \Big(\big(-J_k^{\top}\mathrm{ad}^{\top}_{\mathrm{Ad}_{1k}^{-1}\mu}+\mathcal{A}_l^{\top}\,\mathrm{Ad}_{1k}^{-\top}\mathrm{ad}^{\top}_{\mathrm{Ad}_{1k}^{-1}\mu} \\ &\quad -\tilde{J}_k^{\top}\mathrm{ad}_{\tilde{J}_k\dot{q}}\big)M_k - \tilde{J}_k^{\top}M_k\,\mathrm{ad}_{J_k\dot{q}}\Big)\mathrm{Ad}_{1k}^{-1}.\end{aligned} \tag{85}$$

Upon expanding, followed by invoking Prop. 10 (Appendix A2) for the second term, the matrix $\mathcal{A}_l^{\top}\mathrm{ad}_{\mu}^{\top}M_b$ is obtained. Therefore, (85) is rewritten as in (24).

- Γ_q in (25): The Γ_q matrix in (81d) is expanded as in (25) by simply using (82).

2) Proof of Lemma 10: In the proof, the following identities are used for the block matrix expansions (underbraced parts) of Γ_{qb} and Γ_q, which were obtained in Lemma 9.

$$\begin{aligned}B_1(\dot{q})\mu &= \sum_k \tilde{J}_k^{\top}\big(\mathrm{ad}^{\sim}_{M_k\mathrm{Ad}_{1k}^{-1}\mu}\tilde{J}_k - M_k\mathrm{ad}_{\mathrm{Ad}_{1k}^{-1}\mu}J_k\big)\dot{q} \\ &= B_3(q,\mu)\dot{q}\end{aligned} \tag{86}$$

$$\begin{aligned}\Gamma'_q(\dot{q})\dot{q} &= \sum_k \tilde{J}_k^{\top}\left(-\mathrm{ad}^{\sim}_{M_k\tilde{J}_k\dot{q}}\,\tilde{J}_k + M_k\,\dot{\tilde{J}}_k\right)\dot{q} \\ &= \tilde{\Gamma}'_q(q,\dot{q})\dot{q}\end{aligned} \tag{87}$$

$$\tilde{S}(\mu)^{\top}\mu = \frac{1}{2}\sum_k(\Pi_k^{\top}+\tilde{\Pi}_k)\mu = \frac{1}{2}S(\mu)^{\top}\mu \tag{88}$$

These three identities follow straight forwardly by using (3) and $\mathrm{ad}_X Y = -\mathrm{ad}_Y X$ for rearrangement. Applying these identities to the L.H.S of Lemma 10, we obtain all the terms, but $\tilde{\mathcal{B}} = -(B_2+B_3)$. Expanding $\tilde{\mathcal{B}}$, using $\tilde{J}_k$, and (68d) to cancel terms results in (19e).

H. Lemmas for Controller in Sec V-A

Lemma 15: For body velocities, V_1, V_2, $V_e \in \mathbb{R}^6 \cong \mathfrak{se}(3)$, such that, $V_e = V_1 - V_2$, given inertia $\mathcal{M}$, the following holds,

$$\mathrm{ad}^{\sim}_{\mathcal{M}V_1}V_1 - \mathrm{ad}^{\sim}_{\mathcal{M}V_2}V_2 = \mathrm{ad}^{\top}_{V_1}\mathcal{M}V_1 - \mathrm{ad}^{\top}_{V_2}\mathcal{M}V_2 = \mathcal{C}(V_1,V_e)V_e,$$

where $\mathcal{C}(V_1,V_e) = (\mathrm{ad}^{\top}_{V_1}\mathcal{M} + \mathrm{ad}^{\sim}_{\mathcal{M}V_1} - \mathrm{ad}^{\top}_{V_e}\mathcal{M})$.

Proof: see [25, Lemma 6]. ∎

A useful skew-symmetric operator is defined using $\mathcal{C}$ as,

$$\tilde{\mathcal{C}}(V_1,V_e) = \mathcal{C}(V_1,V_e) - \mathcal{M}\mathrm{ad}_{V_1},\ \tilde{\mathcal{C}}^{\top} = -\tilde{\mathcal{C}}. \tag{89}$$

Lemma 16: (For (56)) Using commutative Prop. 2 for S, P,

$$\begin{aligned}\langle\dot{q},\mu_e\rangle_{\Gamma_2} &= \langle\mu_e,\dot{q}\rangle_{\Gamma_2^{\top}} \\ &= \mu_e^{\top}\big(S(\mu) - (M_b\mathrm{ad}_{\mu} - \mathrm{ad}^{\sim}_{M_b\mu})\mathcal{A}_l\big)\dot{q} \\ &= \mu_e^{\top}\big(P(\dot{q}) + (M_b\mathrm{ad}_{\mathcal{A}_l\dot{q}} + \mathrm{ad}^{\top}_{\mathcal{A}_l\dot{q}}M_b\mu)\big)\mu.\end{aligned} \tag{90}$$

Lemma 17: (For (56)) Using commutative Prop. 2 for S, P,

$$\langle\dot{q},\mu_e\rangle_{2\tilde{S}^{\top}} = \langle\mu_e,\dot{q}\rangle_{2\tilde{S}} = \mu_e^{\top}\big(-P - 2\mathrm{ad}^{\top}_{\mathcal{A}_l\dot{q}}M_b\big)\mu_e. \tag{91}$$

ACKNOWLEDGMENT

The authors thank Dr. Patrick Wensing, University of Notre Dame, for helpful discussions on multibody dynamics.

REFERENCES

[1] G. Garofalo, B. Henze, J. Englsberger, and C. Ott, "On the inertially decoupled structure of the floating base robot dynamics," *IFAC-PapersOnLine*, vol. 48, no. 1, pp. 322 – 327, 2015. 8th Vienna International Conferenceon Mathematical Modelling.

[2] P. J. From, I. Schjølberg, J. T. Gravdahl, K. Y. Pettersen, and T. I. Fossen, "On the boundedness and skew-symmetric properties of the inertia and coriolis matrices for vehicle-manipulator systems," *IFAC Proceedings Volumes*, vol. 43, no. 16, pp. 193 – 198, 2010. 7th IFAC Symposium on Intelligent Autonomous Vehicles.

[3] M. De Stefano, R. Balachandran, A. M. Giordano, C. Ott, and C. Secchi, "An energy-based approach for the multi-rate control of a manipulator on an actuated base," in *2018 IEEE International Conference on Robotics and Automation (ICRA)*, pp. 1072–1077, May 2018.

[4] R. Featherstone, *Rigid Body Dynamics Algorithms*. Berlin, Heidelberg: Springer-Verlag, 2007.

[5] A. Saccon, S. Traversaro, F. Nori, and H. Nijmeijer, "On centroidal dynamics and integrability of average angular velocity," *IEEE Robotics and Automation Letters*, vol. 2, pp. 943–950, April 2017.

[6] J. E. Marsden and J. Scheurle, "The reduced euler-lagrange equations," in *Dynamics and Control of Mechanical Systems: The Falling Cat and Related Problems*, Crm Proceedings & Lecture Notes, American Mathematical Society, 1993.

[7] S. D. Kelly and R. M. Murray, "Geometric phases and robotic locomotion," *Journal of Robotic Systems*, vol. 12, no. 6, pp. 417–431, 1995.

[8] R. L. Hatton and H. Choset, "Geometric motion planning: The local connection, stokes' theorem, and the importance of coordinate choice," *The International Journal of Robotics Research*, vol. 30, no. 8, pp. 988–1014, 2011.

[9] R. Hatton and H. Choset, "Nonconservativity and noncommutativity in locomotion," *The European Physical Journal Special Topics*, vol. 224, pp. 3141–3174, Dec 2015.

[10] J. B. Melli, C. W. Rowley, and D. S. Rufat, "Motion planning for an articulated body in a perfect planar fluid," *SIAM Journal on Applied Dynamical Systems*, vol. 5, no. 4, pp. 650–669, 2006.

[11] R. Mason and J. Burdick, "Propulsion and control of deformable bodies in an ideal fluid," in *Proceedings 1999 IEEE International Conference on Robotics and Automation (Cat. No.99CH36288C)*, vol. 1, pp. 773–780 vol.1, 1999.

[12] E. Shammas, K. Schmidt, and H. Choset, "Natural gait generation techniques for multi-bodied isolated mechanical systems," in *Proceedings of the 2005 IEEE International Conference on Robotics and Automation*, pp. 3664–3669, 2005.

[13] A. M. Bloch, P. S. Krishnaprasad, J. E. Marsden, and R. M. Murray, "Nonholonomic mechanical systems with symmetry," *Archive for Rational Mechanics and Analysis*, vol. 136, pp. 21–99, Dec 1996.

[14] A. M. Giordano, G. Garofalo, M. D. Stefano, C. Ott, and A. Albu-Schäffer, "Dynamics and control of a free-floating space robot in presence of nonzero linear and angular momenta," in *IEEE 55th Conference on Decision and Control (CDC)*, pp. 7527–7534, Dec 2016.

[15] S. Nicosia and P. Tomei, "Robot control by using only joint position measurements," *IEEE Transactions on Automatic Control*, vol. 35, pp. 1058–1061, Sep. 1990.

[16] S. Ramasamy and R. L. Hatton, "The geometry of optimal gaits for drag-dominated kinematic systems," *IEEE Transactions on Robotics*, vol. 35, no. 4, pp. 1014–1033, 2019.

[17] M. De Stefano, H. Mishra, R. Balachandran, R. Lampariello, C. Ott, and C. Secchi, "Multi-rate tracking control for a space robot on a controlled satellite: A passivity-based strategy," *IEEE Robotics and Automation Letters*, vol. 4, pp. 1319–1326, April 2019.

[18] A. De Luca and L. Ferrajoli, "A modified newton-euler method for dynamic computations in robot fault detection and control," in *2009 IEEE International Conference on Robotics and Automation*, pp. 3359–3364, 2009.

[19] G. Garofalo, C. Ott, and A. Albu-Schäffer, "On the closed form computation of the dynamic matrices and their differentiations," in *2013 IEEE/RSJ International Conference on Intelligent Robots and Systems*, pp. 2364–2359, Nov 2013.

[20] S. Echeandia and P. M. Wensing, "Numerical Methods to Compute the Coriolis Matrix and Christoffel Symbols for Rigid-Body Systems," *Journal of Computational and Nonlinear Dynamics*, vol. 16, 07 2021.

[21] J. I. Mulero, "A new factorization of the coriolis/centripetal matrix," *Robotica*, vol. 27, no. 5, p. 689–700, 2009.

[22] H. Mishra, M. De Stefano, A. M. Giordano, and C. Ott, "Output feedback stabilization of an orbital robot," in *2020 59th IEEE Conference on Decision and Control (CDC)*, pp. 1503–1501, 2020.

[23] K. Nanos and E. G. Papadopoulos, "On the dynamics and control of free-floating space manipulator systems in the presence of angular momentum," *Frontiers in Robotics and AI*, vol. 4, p. 26, 2017.

[24] F. Bullo and R. Murray, "Tracking for fully actuated mechanical systems: a geometric framework," *Automatica*, vol. 35, no. 1, pp. 17–34, 1999.

[25] H. Mishra, M. De Stefano, A. M. Giordano, and C. Ott, "A nonlinear observer for free-floating target motion using only pose measurements," in *2019 American Control Conference (ACC)*, pp. 1114–1121, July 2019.

[26] R. M. Murray, "Nonlinear control of mechanical systems: A lagrangian perspective," *Annual Reviews in Control*, vol. 21, pp. 31 – 42, 1997.

[27] S. R. Ploen, "A skew-symmetric form of the recursive newton-euler algorithm for the control of multibody systems," in *1999 American Control Conference (ACC)*, vol. 6, pp. 3770–3773 vol.6, June 1999.

[28] F. Park, J. Bobrow, and S. Ploen, "A lie group formulation of robot dynamics," *The International Journal of Robotics Research*, vol. 14, no. 6, pp. 609–618, 1995.

[29] J. Ostrowski, "Reduced equations for nonholonomic mechanical systems with dissipative forces," *Reports on Mathematical Physics*, vol. 42, no. 1, pp. 185 – 209, 1998. Proceedings of the Pacific Institute of Mathematical Sciences Workshop on Nonholonomic Constraints in Dynamics.

[30] C. Lageman, J. Trumpf, and R. Mahony, "Gradient-like observers for invariant dynamics on a lie group," *IEEE Transactions on Automatic Control*, vol. 55, pp. 367–377, Feb 2010.

[31] A. Beyer, G. Grunwald, M. Heumos, M. Schedl, R. Bayer, W. Bertleff, B. Brunner, R. Burger, J. Butterfaß, R. Gruber, *et al.*, "Caesar: Space robotics technology for assembly, maintenance, and repair," in *Proceedings of the International Astronautical Congress, IAC*, 2018.

[32] O. Itani and E. Shammas, "Motion planning for a redundant planar snake robot," in *2020 IEEE/ASME International Conference on Advanced Intelligent Mechatronics (AIM)*, pp. 1483–1488, 2020.

[33] D. Rollinson, R. L. Hatton, and H. Choset, "Coordinates matter: Virtual chassis and minimum perturbation coordinate representations," in *Adaptive Mobile Robotics*, pp. 183–190.

[34] J. Kim, "Lie group formulation of articulated rigid body dynamics," tech. rep., Technical report, Carnegie Mellon University, 2012.

[35] A. Bloch and B. Brogliato, "Nonholonomic mechanics and control," *Appl. Mech. Rev.*, vol. 57, no. 1, pp. B3–B3, 2004.

Hrishik Mishra is a research associate at the department of *Analysis and Control of Advanced Robotic Systems (ARR)* in the *Institute of Robotics and Mechatronics* of the *German Aerospace Center (DLR)* since 2017. He is also pursuing his doctoral degree with *Technische Universität (TU) Wien, Austria*, under the supervision of Univ.-Prof. Dr. techn. Andreas Kugi and the mentorship of Univ.-Prof. Dr.-Ing. Christian Ott. He received his M.Sc. degree in Satellite Application Engineering from the *Technische Universität (TU) München, Germany*, in 2017 with a specialization in Navigation. Earlier, he received his B.Tech. degree in Electrical and Electronics Engineering from the *Biju Patnaik University of Technology (BPUT), India*, with a specialization in control systems in 2010. His current research activities are directed towards whole-body control, output-feedback control, shared control, and hardware-in-the-loop simulation, especially in the domain of orbital robotic systems.

Gianluca Garofalo is a senior research scientist at *ABB AB, Corporate Research, Sweden*. During 2011-21, he was a research associate at the department of ARR in the *Institute of Robotics and Mechatronics* of DLR. In 2017, he obtained his Ph.D. from the *Technische Universität (TU) München, Germany*, for his work on elastically actuated bipedal robots. His research interests include whole-body and impedance control, bipedal and flexible joint robots, nonlinear robot control and modeling of robotic systems. He is an ICRA and RAL Associate Editor, as well as author of several conference and journal papers.

Alessandro M. Giordano is a research associate at the *Institute of Robotics and Mechatronics* of DLR. He received his Ph.D. from TU München. He received his M.Sc. degree in Astronautical Engineering from *Sapienza Università di Roma, Italy*, in 2014, and his B.Sc. degree in Aerospace Engineering from *Università degli studi di Palermo, Italy*, in 2011. His research interests include space robotics, nonlinear control, flexible multibody dynamics, legged locomotion.

Marco De Stefano received the bachelor's degree in aerospace engineering and the master's degree in astronautical engineering (cum laude) from the *University of Rome La Sapienza, Italy*, in 2008 and 2011, respectively, and the Ph.D. in industrial innovation engineering (summa cum laude) from the *University of Modena and Reggio Emilia, Italy*, in 2019. His Ph.D. has been selected as one of the four finalists of the 2020 Georges Giralt Award for the Best Ph.D. Thesis of Robotics in Europe. Since 2012, he has been a research associate at the department of ARR in the *Institute of Robotics and Mechatronics* of DLR. His research interests include control of space robots, hardware-in-the-loop simulation and stability analysis.

Christian Ott is a Full Professor at TU Wien. He received his Dipl.-Ing. degree in mechatronics from the *Johannes Kepler University (JKU), Linz, Austria*, in 2001 and the Dr.-Ing. degree in control engineering from *Saarland University (SU), Saarbruecken, Germany*, in 2005. During 2001-07, he was a researcher at DLR, and during 2007-09, he was a Project Assistant Professor at the *Department of Mechano-Informatics, University of Tokyo, Japan*. After that, he was a team leader for a *Helmholtz Young Investigators Group* at DLR. During 2014-22 he was the head of the department of ARR in the *Institute of Robotics and Mechatronics* of DLR. He has served as Associate Editor for the IEEE Transactions on Robotics and currently is Co-Editor-in-Chief for IFAC Mechatronics. He was the General Chair of *Humanoids 2020, Munich, Germany*. In 2018, he received an *European Research Council* consolidator grant on energy efficient locomotion for elastic robots. His current research interests include nonlinear robot control, elastic robots, whole-body control, impedance control, and control of humanoid robots.

Andreas Kugi received the Dipl.-Ing. degree in electrical engineering from *Technische Universität (TU) Graz, Austria*, the Ph.D. degree in control engineering and the Habilitation degree in automatic control and control theory from JKU. He was an Associate Professor with JKU during 2000-02 and a Full Professor with SU, during 2002-07. Since 2007, he has been the head of the *Automation and Control Institute (ACIN)*, TU Wien, and since 2017, he is also the Head of the *Center for Vision, Automation & Control at the AIT Austrian Institute of Technology GmbH*. His main research interests include the modeling, control and optimization of complex dynamical systems, the mechatronic system design as well as robotics and process automation. He is full member of the *Austrian Academy of Sciences* and member of the *German National Academy of Science and Engineering (acatech)*.